nature medicine

Cooperative targeting of melanoma heterogeneity with an AXL antibody-drug conjugate and BRAF/MEK inhibitors

Julia Boshuizen[1], Louise A Koopman[2], Oscar Krijgsman[1], Aida Shahrabi[1], Elke Gresnigt–van den Heuvel[2], Maarten A Ligtenberg[1], David W Vredevoogd[1], Kristel Kemper[1], Thomas Kuilman[1], Ji-Ying Song[3], Nora Pencheva[2], Jens Thing Mortensen[2], Marnix Geukes Foppen[1], Elisa A Rozeman[1], Christian U Blank[1], Maarten L Janmaat[2], David Satijn[2], Esther C W Breij[2], Daniel S Peeper[1,5] & Paul W H I Parren[2,4,5]

Intratumor heterogeneity is a key factor contributing to therapeutic failure and, hence, cancer lethality. Heterogeneous tumors show partial therapy responses, allowing for the emergence of drug-resistant clones that often express high levels of the receptor tyrosine kinase AXL. In melanoma, AXL-high cells are resistant to MAPK pathway inhibitors, whereas AXL-low cells are sensitive to these inhibitors, rationalizing a differential therapeutic approach. We developed an antibody-drug conjugate, AXL-107-MMAE, comprising a human AXL antibody linked to the microtubule-disrupting agent monomethyl auristatin E. We found that AXL-107-MMAE, as a single agent, displayed potent *in vivo* anti-tumor activity in patient-derived xenografts, including melanoma, lung, pancreas and cervical cancer. By eliminating distinct populations in heterogeneous melanoma cell pools, AXL-107-MMAE and MAPK pathway inhibitors cooperatively inhibited tumor growth. Furthermore, by inducing AXL transcription, BRAF/MEK inhibitors potentiated the efficacy of AXL-107-MMAE. These findings provide proof of concept for the premise that rationalized combinatorial targeting of distinct populations in heterogeneous tumors may improve therapeutic effect, and merit clinical validation of AXL-107-MMAE in both treatment-naive and drug-resistant cancers in mono- or combination therapy.

Intratumor heterogeneity is a common cause for the lethality of cancer, at least in part because it allows for the accumulation of distinct tumor subsets that are endowed with differential susceptibilities to treatment, whether chemo-, targeted- or immunotherapy-based[1–3]. Indeed, resistance in heterogeneous tumors to single-modality therapies is a common and challenging hurdle in cancer therapy, limiting the benefit of single-agent clinical approaches. To achieve more durable clinical responses, it has been proposed that combination therapies targeting at least two different pathways need to be applied[4]. However, although our understanding of clonal evolution of resistant tumor clones has increased considerably thanks to recent technological advances, our knowledge about tumor heterogeneity is not routinely used to develop rationalized combinatorial treatment regimens.

A disease exemplifying the clinical challenges of intratumor heterogeneity is melanoma. Selective $BRAF^{V600E}$ and MEK inhibitors show marked clinical activities and have transformed the treatment of BRAF-mutant melanoma[5–8]. However, after an initial response, most patients eventually relapse because of the emergence of drug resistance[5–10]. The mechanisms of resistance to MAPK pathway targeted therapy are highly pleiotropic[11–14]. As we and others have shown previously, the diversity of these resistance mechanisms can be observed even in individual patients[15,16]. On the other hand, a common feature of drug-resistant melanomas is that they express high levels of the receptor tyrosine kinase (RTK) AXL[17,18]. This is associated with a so-called phenotype switch from a proliferative to an invasive state, resembling the mesenchymal state in epithelial-to-mesenchymal transition (EMT)[17–21]. AXL-low melanoma cells resemble the epithelial state in EMT, have higher proliferative potential and are generally sensitive to clinically used MAPK pathway inhibitors[17,18].

AXL is also frequently overexpressed in other cancer types, correlating with poor prognosis[22,23] and drug resistance[24,25] in many settings, including EGFR inhibitor-refractory lung cancer[22,26], PI3K inhibitor resistance in head and neck cancer[22], anti-HER2-resistant breast cancer[27], sunitinib-resistant renal cell cancer[28], and ALK inhibitor-resistant neuroblastoma[29]. Furthermore, AXL expression is associated with acquired resistance to traditional therapies, such as chemotherapy and radiotherapy[30–33]. Consistent with the notion that AXL may contribute to tumorigenesis, its depletion or inhibition restores sensitivity to therapy in models of both breast and lung cancer[26,33].

To the best of our knowledge, rational, specific targeting and elimination of distinct populations in heterogeneous tumors has not yet been explored. We hypothesized that differential targeting of AXL-high (MAPK pathway inhibitor-resistant) and AXL-low (MAPK pathway inhibitor-sensitive) tumor cells may act in a cooperative fashion. AXL-107-MMAE is a first-in-class antibody-drug conjugate (ADC) that was developed to treat AXL-positive tumors, and we investigated

[1]Division of Molecular Oncology and Immunology, Oncode Institute, The Netherlands Cancer Institute, Amsterdam, the Netherlands. [2]Genmab, Utrecht, the Netherlands. [3]Division of Experimental Animal Pathology, The Netherlands Cancer Institute, Amsterdam, the Netherlands. [4]Department of Immunohematology & Blood Transfusion, Leiden University Medical Center, Leiden, the Netherlands. [5]These authors contributed equally to this work. Correspondence should be addressed to E.C.W.B. (e.breij@genmab.com) or D.S.P. (d.peeper@nki.nl).

Received 28 March 2017; accepted 15 December 2017; published online 15 January 2018; doi:10.1038/nm.4472

its efficacy in various cancer solid cancer indications, including lung cancer, cervical cancer and melanoma; in the latter setting, AXL-107-MMAE was investigated as a single agent and in combination treatments with MAPK pathway inhibitors. Furthermore, although several mechanisms may account for the accumulation of drug-resistant cells[34–37], for AXL-positive cells it is unclear whether they already pre-exist as drug-resistant reservoirs, evolve on treatment or both. Thus, we also investigated whether AXL-positive cells reside in untreated melanomas, how they evolve amidst bulk AXL-negative cells as a function of therapeutic pressure and whether they can be effectively targeted by AXL-107-MMAE.

RESULTS

AXL is associated with pan-cancer EMT

AXL has previously been suggested to be associated with the EMT of selected tumor indications[22,24,25,29,33,38]. To determine whether this applies to a broader spectrum of cancer types, we mined The Cancer Genome Atlas (TCGA). We applied an EMT signature, comprising 24 genes that are upregulated in epithelial cells and 52 that are upregulated in mesenchymal cells[39], on the pan-cancer TCGA gene expression data cohort of 11,093 patients comprising 32 tumor types. We observed a highly significant association between EMT and *AXL* RNA expression, implying that there is a pan-cancer association between the expression of AXL and EMT (**Fig. 1a**). These results were recapitulated in a large data set of 971 cancer cell lines, which are available from COSMIC[40] (**Supplementary Fig. 1a**). Furthermore, gene set enrichment analysis (GSEA) revealed a highly significant enrichment for mesenchymal genes in AXL-high tumor samples, both in TCGA and COSMIC (**Supplementary Fig. 1b**,**c**). Combined with the knowledge that AXL upregulation is associated with resistance to a range of therapeutic agents across different cancer types[17,22–24,26–29,33,38], we reasoned that targeting AXL-expressing tumor cells may provide a promising strategy for attacking invasive, drug-resistant cancer cell populations.

Generation of an AXL targeting ADC, AXL-107-MMAE

To target AXL-positive tumors, we generated a diverse panel of human monoclonal antibodies that showed dose-dependent binding to AXL, but not to its family members MER and TYRO3 (**Supplementary Fig. 2a**,**b**). We identified AXL antibodies specific for each of the four extracellular AXL domains (**Supplementary Fig. 2a**,**c**), with binding affinities ranging from 63 to 0.33 nM (**Supplementary Table 1**). Although Ig2-, FN1- and FN2-domain-specific antibodies did not compete with the AXL ligand Gas6 for binding, two of the four Ig1-domain-specific antibodies did (**Supplementary Fig. 2d**). To allow efficient targeting of AXL-positive cells in tumors with a Gas6-rich tumor microenvironment[41], the two antibodies that showed competition with Gas6 were not selected for further studies. All AXL antibodies were internalized on target binding (**Supplementary Fig. 2e**), suggesting that AXL might represent a suitable target for an ADC. AXL-specific ADCs were generated by conjugating the human antibody with the microtubule-disrupting agent MMAE through a protease-cleavable valine citrulline linker. The AXL-ADCs induced dose-dependent cytotoxicity in the AXL-positive lung cancer cell line LCLC-103H (**Supplementary Fig. 2f**). Target-dependent cytotoxicity was observed at concentrations of up to 2.5 μg/ml. Unconjugated AXL clones did not inhibit tumor cell viability, indicating that cytotoxicity was MMAE-dependent. In the LCLC-103H xenograft model, therapeutic treatment with a single dose of 1 mg/kg revealed differences in anti-tumor activity in the AXL-ADC panel (**Supplementary Fig. 2g**). Notably, the potency ranking of the AXL-ADCs for *in vitro* cytotoxicity and the anti-tumor activity *in vivo* were not the same, indicating that the antibody characteristics required for optimal cytotoxicity may be different *in vitro* and *in vivo*. The most potent AXL-ADCs *in vivo*, AXL-107-MMAE, AXL-148-MMAE and AXL-733-MMAE, were those with the highest off-rates (**Supplementary Table 1**). Higher off-rates may be associated with better tumor penetration[42]. Comparison of the three best AXL-ADCs in a pancreatic cancer PDX model revealed that AXL-107-MMAE had superior anti-tumor activity (**Supplementary Fig. 2h**,**i**). On the basis of this, we selected AXL-107-MMAE (HuMax-AXL-ADC) as the preferred candidate for further development.

Nonclinical safety profile of AXL-107-MMAE

We explored the nonclinical safety of AXL-107-MMAE in cynomolgus monkeys, the only standard toxicology species for which AXL-107 binding is comparable to that of humans (**Supplementary Fig. 3** and **Supplementary Table 2**). AXL expression was comparable across a wide range of human and cynomolgus monkey tissues (**Supplementary Fig. 4**), with AXL expression being predominantly observed in macrophages in liver and spleen. Moreover, the binding pattern of AXL-107-MMAE to human and cynomolgus monkey tissue sections was highly comparable (**Supplementary Table 3** and **Supplementary Fig. 5**): specific AXL-107-MMAE binding was noted only in mononuclear (Kupffer) cells in both human and cynomolgus monkey liver, and in the splenic cord cells of cynomolgus monkey, but not human. AXL-107-MMAE was well tolerated at doses of up to 6 mg/kg in cynomolgus monkeys, as assessed by clinical observation and standard toxicology criteria, including body weight (**Supplementary Fig. 6**). We observed no changes in liver function, as assessed by measuring liver-associated plasma enzymes, total bilirubin, total protein, albumin and globulin, in cynomolgus monkeys exposed to AXL-107-MMAE (**Supplementary Fig. 7**). Furthermore, no treatment-related histopathological changes in liver, spleen and lung were observed in the animals at 7 d after dosing. Low neutrophil counts were observed by 7–9 d after treatment with doses of 3 mg/kg or higher, but this was reversible and neutrophil counts generally returned to normal by the time of next treatment, 3 weeks later (**Supplementary Fig. 8**). This nonclinical safety profile is consistent with what can be expected from an MMAE-based ADC[43], with no indication of AXL-specific toxicity. These results support the initiation of a first-in-human dose-escalation study for various solid cancer indications (NCT02988817).

AXL-107-MMAE efficiently induces AXL-specific and MMAE-mediated cytotoxicity *in vitro*

AXL-107-MMAE showed marked cytotoxic activity in tumor cell lines derived from a variety of cancer types. *In vitro* sensitivity to AXL-107-MMAE (IC_{50} values in the range of 0.02–2 μg/ml) correlated with AXL expression, with strong activity requiring AXL cell surface expression of at least 10,000–30,000 molecules per cell (**Fig. 1b**). Some cell lines with high levels of cell-surface AXL lacked sensitivity to AXL-107-MMAE (for example, NCI-H1299). This was not a result of differences in either receptor internalization (**Supplementary Fig. 2j**) or lysosomal degradation (**Supplementary Fig. 2k**). Instead, these cells showed reduced sensitivity to free MMAE (**Supplementary Fig. 2l**), owing to multi-drug resistance gene 1 (*MDR1*) expression[44,45] (**Supplementary Fig. 2m**,**n**,**o**). These results indicate that sensitivity to AXL-107-MMAE is determined primarily by AXL cell-surface expression levels.

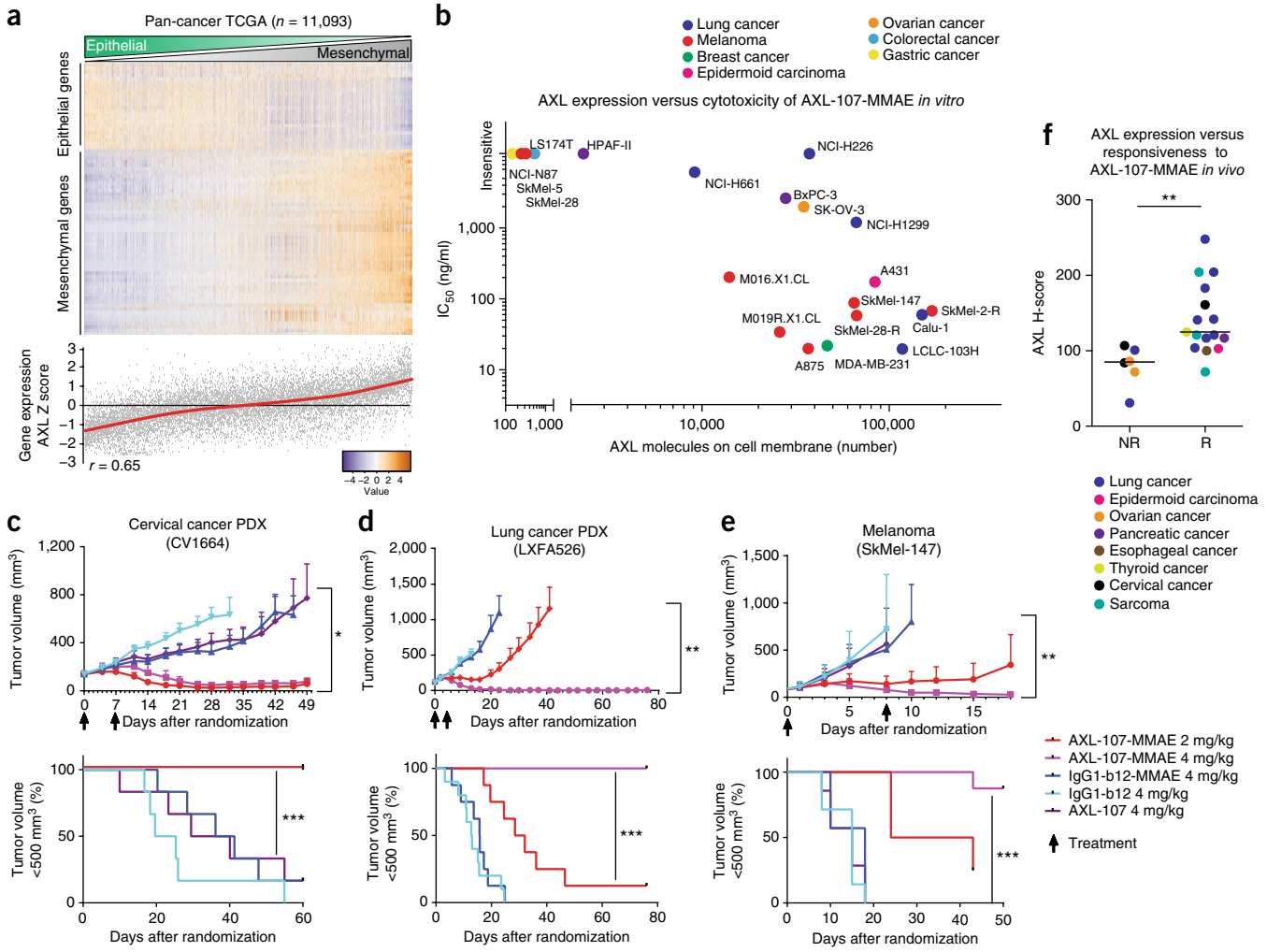

Figure 1 AXL-107-MMAE induces cytotoxicity *in vitro* and *in vivo*. (**a**) Correlation between AXL and EMT gene expression signature profiles of 32 tumor types representing the 11,093 patients available in TCGA. Red line represents locally estimated scatterplot smoothing (LOESS) fit. Statistical analysis was carried out using Pearson's correlation = 0.65 ($P < 0.001$). (**b**) Potency of AXL-107-MMAE, expressed as IC_{50}, was determined in cytotoxicity assays in relation to the number of AXL molecules expressed on the cell membrane, as measured by quantitative flow cytometry. For cell lines that were insensitive to AXL-107-MMAE, the IC_{50} value was arbitrarily set at 10,000 ng/ml. The origin of tumor cell lines is indicated in colors. Statistical analysis was carried out using Pearson's correlation = 0.51 ($P < 0.001$). (**c**–**e**) *In vivo* tumor growth curves and corresponding Kaplan–Meier curves of cervical (**c**, CV1664) and lung (**d**, LXFA526) cancer PDX models and a cell line-derived melanoma (**e**, SkMel-147) model. Arrows indicate antibody injections. IgG1-b12-MMAE and IgG1-b12 were used as conjugated and unconjugated isotype control antibodies, respectively. In addition, AXL-107 was assessed as an unconjugated control antibody. Data points represent average tumor volume, error bars represent s.d. (**c**) $*P < 0.05$, 4 mg/kg AXL-107-MMAE versus IgG1-b12-MMAE (Kruskal–Wallis test combined with Dunn's test on day 32). The difference between the unconjugated AXL-107 and IgG1-b12 treatment was not statistically significant. $***P < 0.005$, 2 and 4 mg/kg showed improved survival compared with control groups (log-rank Mantel–Cox test). $n = 6$ per group. (**d**) $**P < 0.01$; 2 and 4 mg/kg AXL-107-MMAE versus IgG1-b12-MMAE (Mann–Whitney test on day 23). $***P < 0.005$, 2 and 4 mg/kg AXL-107-MMAE showed better survival than control groups (log-rank Mantel–Cox test). $n = 8$ per group. (**e**) $**P < 0.01$, 2 and 4 mg/kg AXL-107-MMAE versus IgG1-b12-MMAE (Mann–Whitney test on day 19). $***P < 0.005$, 2 and 4 mg/kg AXL-107-MMAE showed better survival than control groups (log-rank Mantel–Cox test). $n = 7$ per group. (**f**) AXL expression levels in xenograft tissues, as assessed by immunohistochemistry (H score, as determined by digital pathology/Definiens quantitation, Online Methods). Response (R) is defined as statistically significant growth inhibition and/or regression compared with control IgG1-b12-MMAE. $**P < 0.01$, Mann–Whitney Test. NR, non-response. The origin of tumor cell lines is indicated by color.

AXL-107-MMAE induces MMAE-mediated anti-tumor efficacy *in vivo*

The *in vivo* activity of AXL-107-MMAE was then evaluated in additional cell line-derived and patient-derived xenograft (PDX) models representing different cancer types, including pancreas, esophageal, lung, thyroid, ovarian, cervical cancer, melanoma and sarcoma. AXL-107-MMAE treatment (but not the isotype control ADC IgG1-b12-MMAE) caused tumor regression or tumor growth inhibition in 18 of 25 tumor models (three examples of cervical cancer PDX, lung cancer PDX and melanoma are shown in **Fig. 1c**–**e**). As observed *in vitro*, unconjugated AXL-107 did not inhibit tumor growth, again indicating that anti-tumor activity was mediated by MMAE. To determine whether the correlation between AXL-107-MMAE efficacy and AXL expression that we observed *in vitro* (**Fig. 1b**) could be recapitulated *in vivo*, we performed immunohistochemistry (IHC) on 22 of these models and found that AXL expression scores were significantly

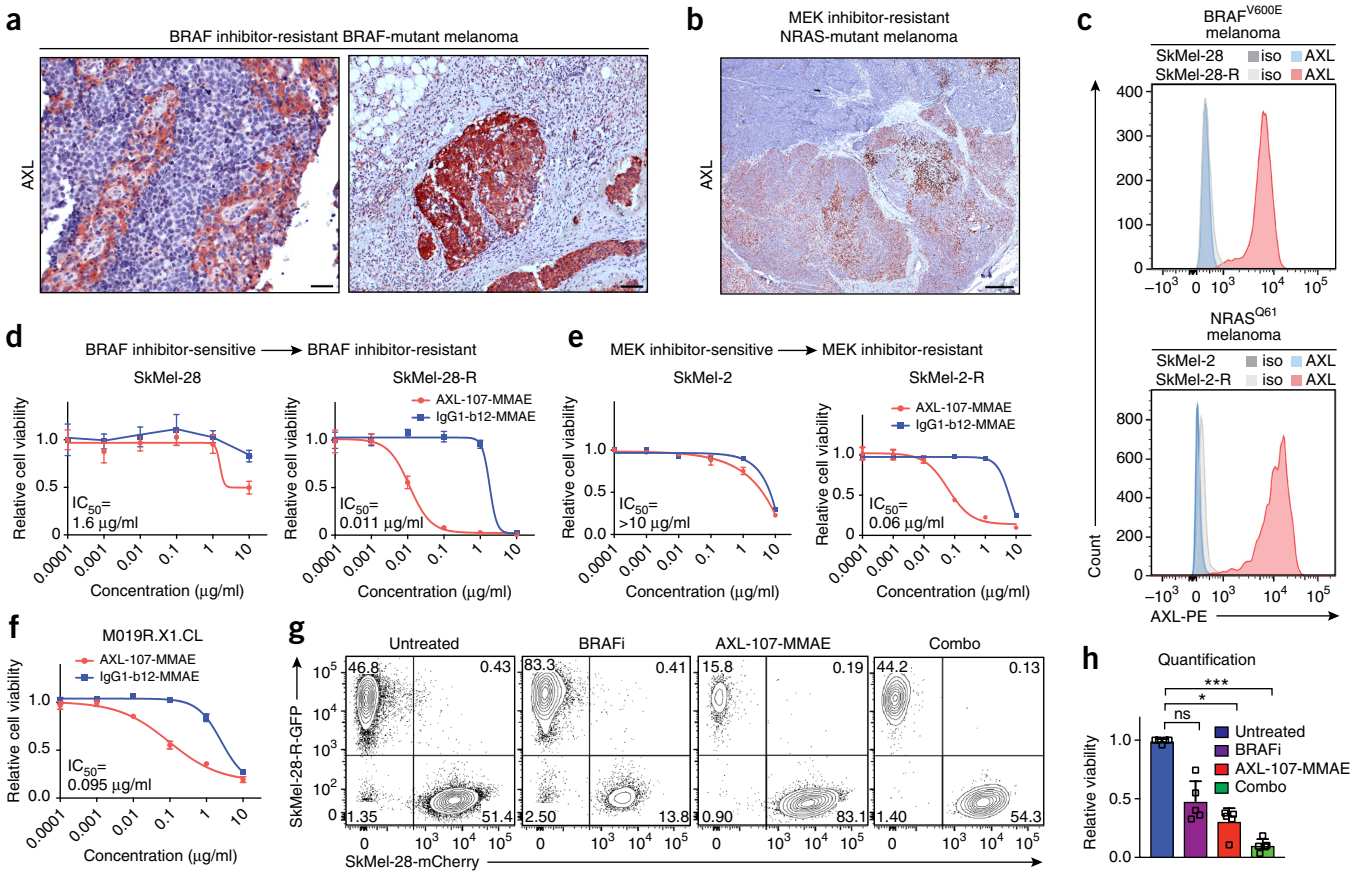

Figure 2 Elimination of distinct tumor populations by AXL-107-MMAE and MAPK pathway inhibition. (**a**) Representative immunohistochemistry for AXL expression on two human BRAF-mutant melanomas that clinically progressed on BRAF inhibitor. Scale bars represent 50 µm (left) and 100 µm (right). (**b**) Representative IHC of AXL expression on human NRAS-mutant melanoma that clinically progressed on MEK inhibitor. Scale bar represents 500 µm. (**c**) Flow cytometric analysis of AXL surface expression of two paired melanoma cell lines; cell lines with 'R' indicate BRAF (SkMel-28-R) or MEK inhibitor (SkMel-2-R) resistance. AXL staining of the parental cell line is shown in blue and the corresponding resistant line in red. Iso (gray) designates staining with an isotype control antibody. Representative images of three independent experiments. (**d**–**f**) Dose response of AXL-107-MMAE (red) versus control IgG1-b12-MMAE (blue) in BRAF-mutant and NRAS-mutant cell lines resistant to BRAF and/or MEK inhibitors. Representative images of three independent experiments. Error bars represent s.d. of three technical replicates. IC_{50} values are indicated in the graphs. (**g**) Flow cytometric analysis of pools of equal numbers of SkMel-28-mCherry and SkMel-28-R-GFP cells treated with AXL-107-MMAE and/or the BRAF inhibitor PLX4720 (BRAFi). Representative images of five independent experiments. (**h**) Quantification of cell count in **g**. Error bars represent s.d. from five independent replicates. Statistical analysis by Kruskal–Wallis; $*P < 0.05$, $***P < 0.001$.

higher in models responding to AXL-107-MMAE than in models that were unresponsive (**Fig. 1f**), confirming the *in vitro* responses and reinforcing the notion that AXL expression is essential for the activity of AXL-107-MMAE.

AXL-107-MMAE eliminates treatment-resistant BRAF- and NRAS-mutant melanomas *in vitro*

We and others have recently reported that melanomas that have acquired resistance to MAPK pathway inhibition commonly express high levels of AXL[17,18] (**Fig. 2a** and **Supplementary Fig. 9a**). Extending these observations, we found that NRAS-mutant melanomas that had progressed on MEK inhibitor treatment also showed marked AXL expression (**Fig. 2b** and **Supplementary Fig. 9a**).

These results prompted us to investigate the efficacy of AXL-107-MMAE in tumors that have acquired resistance to the clinically relevant BRAF and MEK inhibitor combination[5,6,8,46]. We previously generated a BRAF inhibitor-resistant melanoma cell line (SkMel-28-R) from a sensitive parental cell line (SkMel-28) by continuous exposure to BRAF inhibitor[17]. Similarly, we created a MEK inhibitor-resistant cell line (SkMel-2-R) from the NRAS-mutated SkMel-2 cell line. Cell-surface AXL expression was strongly upregulated in both paired cell lines following acquisition of resistance to these MAPK pathway inhibitors, as assessed by flow cytometry (**Fig. 2c**). AXL-107-MMAE, in contrast with isotype control ADC, induced killing of SkMel-28-R and SkMel-2-R *in vitro* (**Fig. 2d**,**e**). As expected, their parental MAPK pathway inhibitor-sensitive counterparts were unresponsive to AXL-107-MMAE, consistent with the fact that these cells express low levels of AXL (**Fig. 2c**). Knockdown of AXL using either of two different shRNAs in SkMel-28-R resulted in a loss of sensitivity to AXL-107-MMAE (**Supplementary Fig. 9b**,**c**), confirming that AXL expression is required for the cytotoxic activity of AXL-107-MMAE. Furthermore, a low-passage PDX cell line, M019R.X1.CL, derived from a vemurafenib-resistant melanoma patient, was sensitive to AXL-107-MMAE (**Fig. 2f**). A variety of other melanoma cell lines with different mutational backgrounds also showed sensitivity to AXL-107-MMAE (**Supplementary Table 4**). Taken together, we conclude

that AXL-107-MMAE eliminates both treatment-naive (**Fig. 1**) and therapy-resistant (**Fig. 2**) melanoma cells *in vitro*.

Elimination of distinct tumor populations by AXL-107-MMAE and MAPK pathway inhibition

Our IHC analyses revealed that AXL-positive tumor cells commonly occur in strongly heterogeneous patterns in drug-resistant melanomas (**Fig. 2a**,**b**). We and others previously reported that AXL-negative melanoma cells are sensitive to BRAF pathway inhibition[17,18]. This provides a rationale for using a combination treatment protocol in which the AXL-negative cells are killed by BRAF pathway inhibition and the AXL-positive cells are eliminated by AXL-107-MMAE. We therefore modeled melanoma intratumor heterogeneity *in vitro* to investigate the potential of AXL-107-MMAE to selectively target an AXL-high population amidst low AXL-expressing cells. We stably transduced SkMel-28 and SkMel-28-R cells with lentiviral vectors to generate mCherry- and GFP-tagged derivatives, respectively. We mixed the cell lines in a 1:1 ratio and treated them for 5 d with either AXL-107-MMAE, BRAF inhibitor or a combination of both. Whereas AXL-107-MMAE specifically eradicated AXL-high cells, BRAF inhibitor selectively reduced the AXL-low population (**Fig. 2g**,**h**). A combination of AXL-107-MMAE and BRAF inhibitor effectively eliminated both populations. Our findings indicate that by targeting distinct melanoma populations, AXL-107-MMAE complements MAPK inhibitor treatment, resulting in a more potent treatment response.

AXL-positive cells are identified in human melanomas before treatment and accumulate on acquisition of drug resistance

Triggered by our initial finding of substantial and common heterogeneity of AXL expression in BRAF and MEK inhibitor-resistant melanomas (**Fig. 2a**,**b** and **Supplementary Fig. 9a**), we evaluated AXL expression by IHC in a cohort of paired melanomas obtained from patients before treatment and following the development of resistance to BRAF and/or MEK inhibitors. These included paired samples derived from individual patients with a BRAF-mutant melanoma treated with the BRAF inhibitor vemurafenib or the combination of BRAF and MEK inhibitors (dabrafenib + trametinib). Furthermore, we analyzed samples from patients with NRAS-mutant melanoma who received MEK inhibitor (trametinib) treatment.

We found that AXL-positive tumor cells were commonly present in untreated melanomas. Even in largely AXL-negative melanomas, we observed either single or small groups of AXL-positive cells in the vast majority of pre-treatment tumors, including both $BRAF^{V600E}$ (five of six) and $NRAS^{Q61}$ (seven of eight) melanomas (**Fig. 3a**,**b**). Furthermore, we observed an increase in AXL expression in five of seven patients with BRAF-mutant melanomas who relapsed on treatment with either a BRAF inhibitor or the combination of BRAF and MEK inhibitors (**Fig. 3c**). In paired samples from three patients with NRAS-mutated melanomas who relapsed on MEK inhibition, two samples showed an increase in AXL expression. These results indicate that AXL is commonly upregulated not only in BRAF-mutant melanomas following acquisition of resistance to BRAF (+MEK) inhibitors, but also in NRAS-mutant melanomas treated with a MEK inhibitor.

We recently established a large platform of patient-derived melanoma xenograft (PDX) models that were derived from untreated and MAPK-pathway-inhibitor-refractory patients[47]. To enable translational studies, we determined whether the small populations of AXL-positive cells that we frequently identified in patients' melanomas were also present in PDX tumor tissues. IHC of a panel of pre-treatment PDX revealed common AXL-positive cells (**Fig. 3d**). From this PDX platform, we also derived low-passage cell lines, including those harboring either a $BRAF^{V600E}$ or $NRAS^{Q61}$ mutation, which were subjected to immunoblotting and flow cytometry for AXL. Consistent with what we observed for both patients' samples and PDX, we also detected AXL in untreated PDX cell lines (**Fig. 3e**). Furthermore, we observed upregulation of AXL following acquisition of resistance in paired PDX cell lines obtained from two individual patients before treatment and after relapse on vemurafenib (**Fig. 3e**). Flow cytometric analyses confirmed cell-surface expression of AXL on PDX-derived cell lines (**Supplementary Fig. 9d**). These data not only confirm that AXL is commonly upregulated in therapy-resistant melanomas, but also show that AXL-positive cells already exist before treatment in heterogeneous tumors.

AXL-positive cells are rapidly selected following therapeutic pressure

The presence of pre-treatment AXL-positive cells raises the possibility that these cells represent a pre-existing drug-resistant reservoir that is selected for, and expands, under therapeutic pressure. To test this hypothesis, we modeled the fate of sporadic AXL-positive cells amidst a bulk of AXL-negative cells as a function of treatment. We admixed BRAF inhibitor-resistant, AXL-high SkMel-28-R-GFP cells with drug-sensitive, AXL-low SkMel-28-mCherry cells in a 1:1,000 ratio and exposed them to BRAF inhibitor. Although the population ratio remained similar in the absence of treatment, therapeutic pressure by BRAF inhibition caused a marked shift in which the rare AXL-positive cells expanded to comprise over 90% of the total cell population in as little as 3 weeks (**Fig. 3f**). Similarly, AXL-low, MEK inhibitor sensitive cells were replaced by AXL-high, MEK-inhibitor-resistant cells following treatment with MEK inhibitor (**Supplementary Fig. 9e**). Taken together, these results suggest that rare pre-treatment AXL-expressing cells are strongly selected for when challenged with MAPK pathway inhibitors, eventually producing large populations of AXL-positive cells that contribute to the relapse of melanomas, whether carrying a BRAF or NRAS mutation. Consistent with this notion, we observed that the few SkMel-28 cells that persisted through the treatment (**Fig. 3f**) were highly resistant to BRAF inhibitor (**Fig. 3g**). Corroborating our model, this BRAF inhibitor-refractory cell fraction showed increased susceptibility to elimination by AXL-107-MMAE (**Fig. 3h**).

Acute transcriptional upregulation of AXL following MAPK pathway inhibition

Our results indicate that AXL-expressing cells are enriched following acquisition of resistance to MAPK inhibition. We next investigated whether targeted inhibitors also have an immediate effect on AXL expression. Indeed, for PDX cell lines and a number of commonly used melanoma cell lines, we observed a strong increase in cell-surface AXL protein expression after 3–10 d of treatment with BRAF and/or MEK inhibitors (**Fig. 4a**,**b** and **Supplementary Fig. 10a**,**b**). This was observed in $BRAF^{V600E}$ melanoma cell lines when exposed to BRAF and MEK inhibitors and in $NRAS^{Q61}$ melanoma cell lines following treatment with MEK inhibitor. *AXL* mRNA levels sharply increased after treatment with BRAF and/or MEK inhibitors, indicating that this effect occurred at the transcriptional level (**Fig. 4c** and **Supplementary Fig. 10c**). We conclude that the enhanced AXL levels that are characteristic of relapsed drug-treated melanomas accumulate by at least two distinct processes: an increase of pre-existing subpopulations of AXL-expressing cells and acute transcriptional induction of AXL expression by drug treatment.

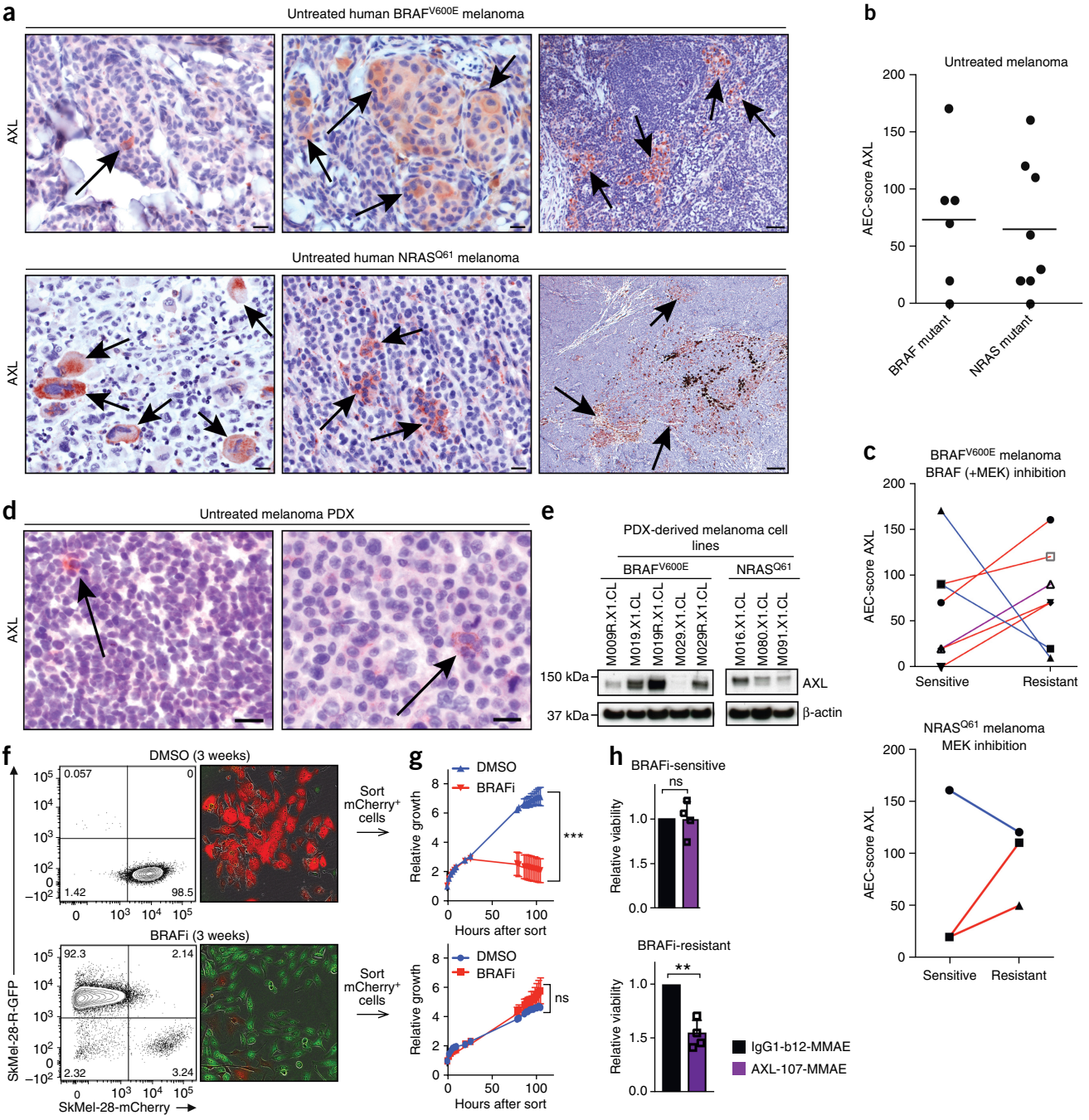

Figure 3 AXL-positive cells reside in pre-treatment melanomas and rapidly outgrow bulk AXL-negative cells following therapeutic pressure. (**a**) Representative immunohistochemical staining for AXL expression on biopsies from melanoma patients before therapy. Arrows indicate single and groups of AXL-positive cells. Scale bars represent 20 μm (left and middle) and 100 μm (right). (**b**) AXL expression by immunohistochemistry in the untreated melanoma cohort stratified for BRAF or NRAS mutation, quantified as 3-amino-9-ethylcarbazole (AEC) H-score (Online Methods). (**c**) Paired patient melanoma samples before the start of therapy (all sensitive) and after acquiring resistance. Lines connect paired samples. Red represents AXL up ($n = 6$) and blue AXL down ($n = 3$) following resistance to BRAF or MEK inhibitor treatment alone. The purple line (triangles; $n = 1$) indicates a BRAF ^{V600E} melanoma sample before and after resistance to a combination of BRAF and MEK inhibitors. (**d**) Immunohistochemical staining for AXL on PDX-derived untreated melanomas. Arrows indicate AXL-positive cells. Scale bar represents 20 μm. (**e**) Western blot analysis of BRAF^{V600E} PDX-derived melanoma cell lines, including paired samples from patient M019 and M029 before the start of treatment with the BRAF inhibitor vemurafenib and after relapse (indicated in cell lines with 'R'), and of NRAS^{Q61} PDX-derived melanoma cell lines. Full blot is shown in **Supplementary Figure 12.** (**f**) Flow cytometric analysis of pools of 1,000:1 SkMel-28-mCherry:SkMel-28-R-GFP cells treated with control (DMSO alone) or BRAF inhibitor for 3 weeks. Right, representative images from corresponding flow cytometry plots at the time of harvest of the cells. Representative images of three independent experiments. (**g**) FACSorted SkMel-28-mCherry cells from **f** were re-plated and live-cell imaged. Cells were treated with BRAF inhibitor or DMSO (control) for 3 d. Error bars represent s.d. of two technical replicates. Representative graphs of two independent experiments. Statistical analysis was carried out using Mann–Whitney; ***$P < 0.001$, ns = not significant. (**h**) Relative viability of SkMel-28-mCherry cells sorted after 3 weeks of treatment with BRAF inhibitor or control from **f** and **g** and sequentially subjected to AXL-107-MMAE for 5 d. Pooled data from two independent experiments with two technical replicates each. Statistical analysis by Mann–Whitney; **$P < 0.01$, ns = not significant.

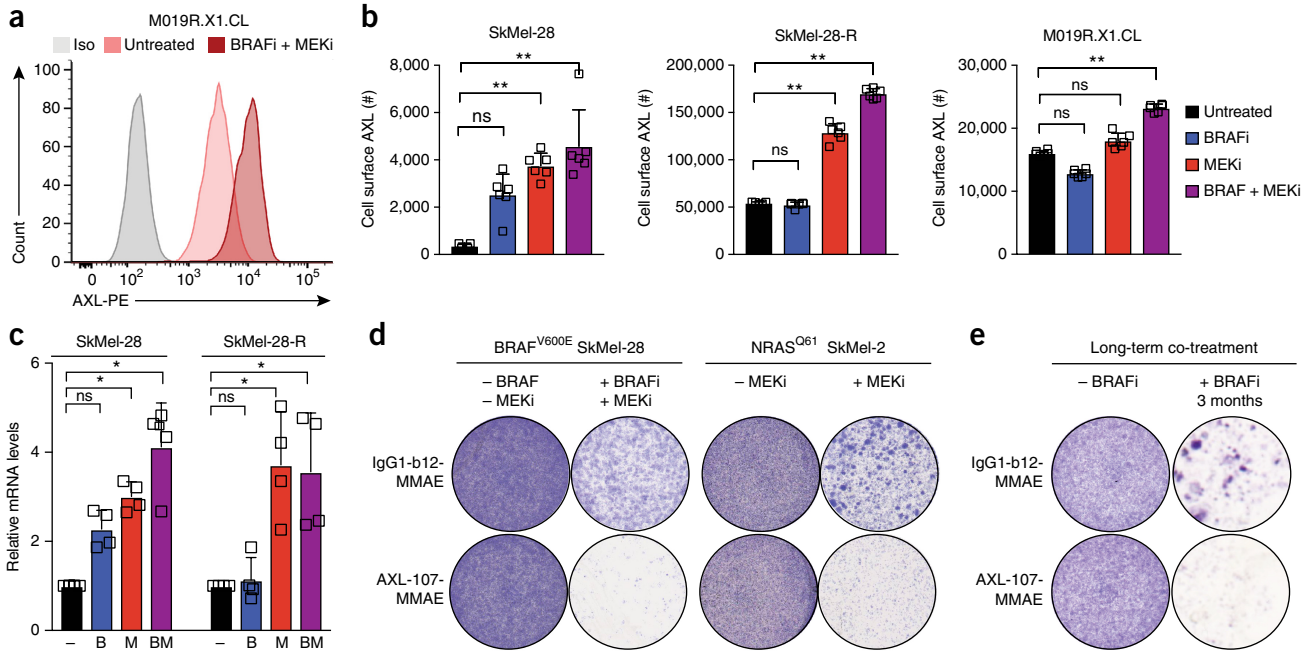

Figure 4 AXL-107-MMAE and MAPK inhibitors mutually potentiate cytotoxicity. (**a**) Flow cytometric image of M019R.X1.CL cells treated with indicated compounds for 3 d and stained for AXL. Representative image of three independent experiments. (**b**) Flow cytometric analysis of AXL expression and cell surface quantification of AXL on three cell lines, including a PDX-derived cell line, in response to BRAF and/or MEK inhibitor; treatment for 3 d. Error bars represent s.d. of six independent replicates. In SkMel-28, untreated cells were below detectable limits of assay (<3,300). Statistical analysis by Kruskal–Wallis; $^{**}P < 0.01$, ns = not significant. (**c**) mRNA levels of AXL following treatment with the indicated compounds (– = untreated, B = BRAFi, M = MEKi, BM = BRAFi + MEKi) for 3 d. RPL13 was used as internal control for quantification. Error bars represent s.d. of four independent replicates. Statistical analysis performed by Kruskal–Wallis; $^{*}P < 0.05$, ns = not significant. (**d**) Colony formation assay of cell lines treated with BRAF and/or MEKi and/or AXL-107-MMAE versus control ADC for 5 d. Representative image of three independent replicates. (**e**) Colony formation assay of SkMel-28 treated with BRAF inhibitor for 3 months with AXL-107-MMAE or control ADC. Representative image of three independent experiments.

AXL-107-MMAE and MAPK inhibitors mutually potentiate cytotoxicity *in vitro*

Although the results shown in **Figure 2** indicate that AXL-positive MAPK inhibitor-resistant melanoma cells are effectively eliminated by AXL-107-MMAE, the results shown in **Figure 4** suggest that the acute induction of AXL expression by MAPK pathway inhibition might be exploited to target cancers with initially low baseline AXL levels. Treatment of several AXL-low melanoma cell lines with AXL-107-MMAE alone had little effect (**Fig. 4d** and **Supplementary Fig. 10d**). In contrast, combined treatment with BRAF and/or MEK inhibitors caused cooperative elimination. This effect was observed irrespective of whether these cells were driven by mutant BRAF or NRAS.

Extending these findings, we determined whether AXL-107-MMAE is also capable of preventing the emergence of BRAF inhibitor-resistant clones. We treated the AXL-low cell line SkMel-28 for 3 months with BRAF inhibitor, either alone or in combination with AXL-107-MMAE. As expected, single-agent BRAF inhibitor failed to prevent the outgrowth of resistant cell groups (**Fig. 4e** and **Supplementary Fig. 10e**). In contrast, co-treatment with AXL-107-MMAE strongly suppressed the emergence of drug-resistant clones. This result indicates that AXL-107-MMAE and MAPK inhibitors potentiate each other's efficacy to cooperatively prevent outgrowth of resistant tumor cell colonies.

AXL-107-MMAE and MAPK pathway inhibitors cooperatively inhibit melanoma PDX growth

These results demonstrate that, *in vitro*, AXL-107-MMAE and MAPK pathway inhibitors cooperate to eliminate melanoma cells. Thus, we set out to validate these results in our panel of melanoma PDX models *in vivo*[47]. Based on these results, we identified two groups of melanomas that are likely to respond to AXL-107-MMAE, either alone or in combination with MAPK pathway inhibition: AXL-high, BRAF inhibitor-resistant tumors in a single-agent AXL-107-MMAE setting, and AXL-low or heterogeneous tumors in a combination setting with MAPK pathway inhibition; both models were studied accordingly.

First, we set up a subcutaneous xenograft model in mice with the PDX-derived cell line M019R.X1.CL, which originated from a patient with a tumor that was intrinsically resistant to vemurafenib and expressed high levels of AXL (**Supplementary Figs. 11a** and **12**). This tumor displayed cross-resistance to the combination of dabrafenib and trametinib *in vivo* (**Fig. 5a**). As expected, this melanoma was highly susceptible to elimination by AXL-107-MMAE, demonstrating the potential of AXL-107-MMAE to target MAPK inhibition-resistant melanoma as a single agent. In view of the further induction of AXL following MAPK pathway inhibition (**Fig. 4a**,**b**), we also determined whether the triple combination comprising BRAF and MEK inhibitors and AXL-107-MMAE would yield increased tumor inhibition. To investigate this, we stratified the BRAF and MEK inhibitor-treated tumors into three groups at the end of the initial experiment and subsequently treated them with either BRAF and MEK inhibitors, BRAF and MEK inhibitors and AXL-107-MMAE, or AXL-107-MMAE monotherapy. Although switching to AXL-107-MMAE monotherapy prolonged the survival of these mice relative to MAPK pathway inhibition, the best survival benefit was observed for the triple combination treatment (**Fig. 5b** and **Supplementary Fig. 11b**).

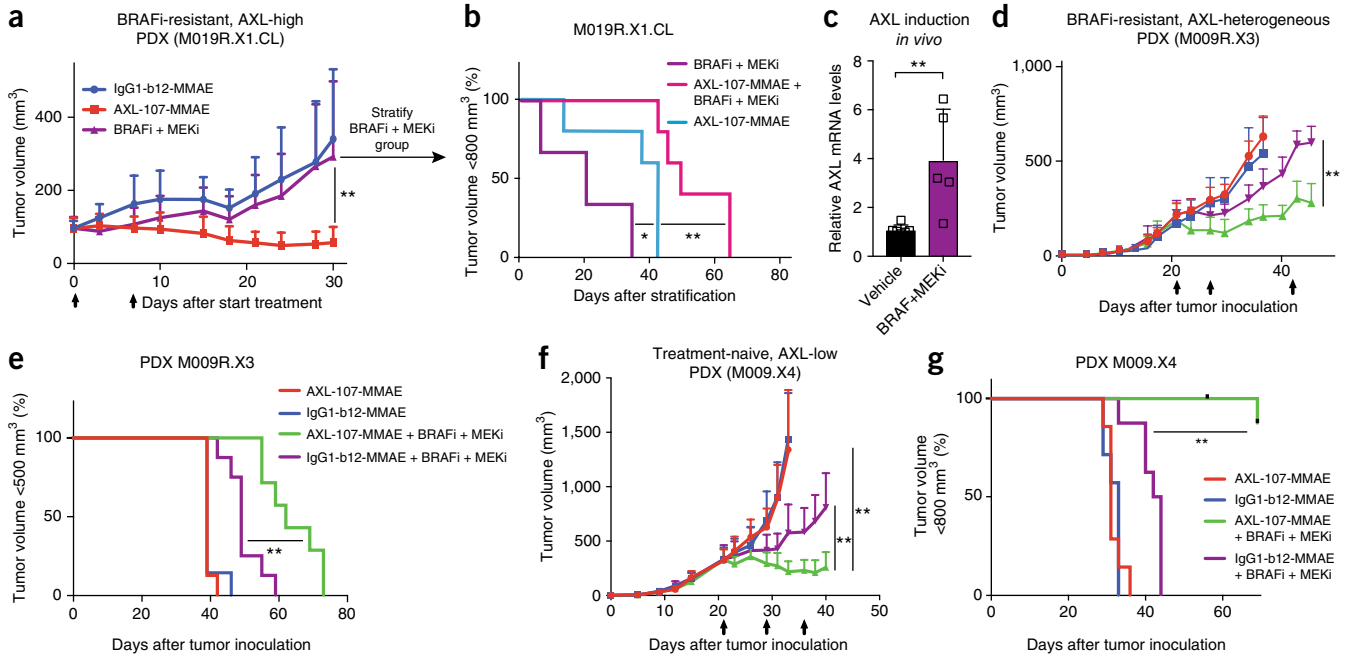

Figure 5 AXL-107-MMAE and MAPK pathway inhibitors cooperatively inhibit melanoma PDX growth. (**a**) Tumor growth curve of PDX-derived melanoma cell line M019R.X1.CL and treatment with AXL-107-MMAE ($n = 8$) versus control IgG1-b12-MMAE ($n = 8$) versus BRAF and MEK inhibition ($n = 13$). Error bars represent s.d. Arrows indicate compound injections 0 and 7 d after treatment start. Oral gavage of BRAF and MEK inhibitor started on day 0 and was given daily. Statistical analysis was carried out using Kruskal–Wallis test; $^{**}P < 0.01$. (**b**) Kaplan–Meier survival curve of M019R.X1.CL mice treated with BRAF and MEK inhibitor and re-stratified into three groups as indicated ($n = 3$ in BRAF + MEKi group, $n = 5$ in other two groups). Statistical analysis by log-rank Mantel–Cox test; $^{*}P < 0.05$, $^{**}P < 0.01$. (**c**) mRNA AXL levels in PDX M009R.X3 tumor tissue following BRAF + MEK inhibition for 7 d *in vivo*. Error bars represent s.d. Average of five tumors is shown. Statistical analysis by Mann–Whitney; $^{**}P < 0.01$. (**d**) Tumor growth curve of PDX M009R.X3 following treatment with indicated compounds ($n = 7$ in AXL-107-MMAE + BRAF + MEKi group, $n = 8$ in all other groups). Error bars represent s.d. Arrows indicate ADC injections on days 20, 27 and 42. Oral gavage of BRAF+MEK inhibitor started on day 20 for the relevant groups and was given daily. Statistical analysis by Kruskal–Wallis test; $^{**}P < 0.01$. (**e**) Kaplan–Meier survival curves of M009R.X3 following treatment as indicated. Statistical analysis by log-rank Mantel–Cox test; $^{**}P < 0.01$. (**f**) Tumor growth curve of PDX M009.X4 following treatment with indicated compounds ($n = 7$ in AXL-107-MMAE and IgG1-b12-MMAE groups, $n = 8$ in IgG1-b12-MMAE + BRAF + MEKi group, $n = 9$ in AXL-107-MMAE + BRAF + MEKi group). Error bars represent s.d. Arrows indicate weekly ADC injections starting on day 21. Oral gavage of BRAF and MEK inhibitor started on day 21 and was given daily. Statistical analysis was carried out using Kruskal–Wallis test; $^{**}P < 0.01$. (**g**) Kaplan–Meier survival curves of M009.X4 following treatment as indicated. Statistical analysis by log-rank Mantel–Cox test; $^{**}P < 0.01$.

Second, we determined whether a combination strategy consisting of AXL-107-MMAE and BRAF and MEK inhibitors could be exploited therapeutically in AXL-heterogeneous or even AXL-low tumors. For one setting, we used melanoma PDX M009R.X3, which was derived from a patient who had progressed on vemurafenib. This tumor is heterogeneous for AXL expression *in vivo* (**Supplementary Fig. 11a,d**), consistent with our previous[17] and current (**Fig. 3c** and **Supplementary Fig. 9a**) observations that not all therapy-resistant melanomas are homogeneously AXL high. We observed an acute induction in AXL expression following treatment with BRAF and MEK inhibitors *in vivo* (**Fig. 5c** and **Supplementary Fig. 11c**), in keeping with our *in vitro* observations (**Supplementary Fig. 10a**). Consistent with this notion, AXL-107-MMAE treatment significantly augmented the extent of tumor inhibition by BRAF and MEK inhibition (**Fig. 5d**), allowing for increased survival (**Fig. 5e**).

To explore yet another model that could benefit from the acute induction of AXL following MAPK pathway inhibition, we implanted the treatment-naive, patient-matched counterpart of PDX M009R.X3, M009.X4, in mice. This AXL-low tumor (**Supplementary Fig. 11a**) displayed no sensitivity to AXL-107-MMAE as a single agent, as expected (**Fig. 5f**). Although BRAF and MEK inhibitors partially controlled tumor growth, the addition of AXL-107-MMAE greatly enhanced tumor inhibition, leading to increased overall survival (**Fig. 5g**). Taken together, these *in vivo* PDX results demonstrate that AXL-107-MMAE and MAPK pathway inhibitors cooperatively inhibit melanoma growth for both treatment-naive and BRAF and MEK inhibitor-resistant melanomas.

DISCUSSION

We found that the presence of high levels of AXL in both untreated and resistant tumors is a trait that is amenable to therapeutic intervention. ADCs represent a powerful approach to eliminate cells using a target of interest as a vehicle to transfer highly toxic molecules into cells[48–50]. We describe the development of AXL-107-MMAE, a new AXL ADC that specifically targets AXL-expressing tumor cells across a broad range of cancer types. Notably, with this approach, AXL is used as an address for the ADC to deliver its toxic cargo in cells expressing sufficient levels of AXL on their surface, rather than as a target for intracellular signaling inhibition. Thus, AXL-107-MMAE eliminates cancer cells independently of AXL-mediated signaling for cell growth or survival. Furthermore, MMAE has the potential to generate bystander toxicity, a process in which surrounding tumor cells can be eliminated by free MMAE that is released from target-positive tumor cells that have processed the ADC[51,52]. We observed strong anti-tumor activity of AXL-107-MMAE as single-agent therapy in AXL-high PDX models covering a plethora of solid cancer types, including lung and cervical cancer and melanoma.

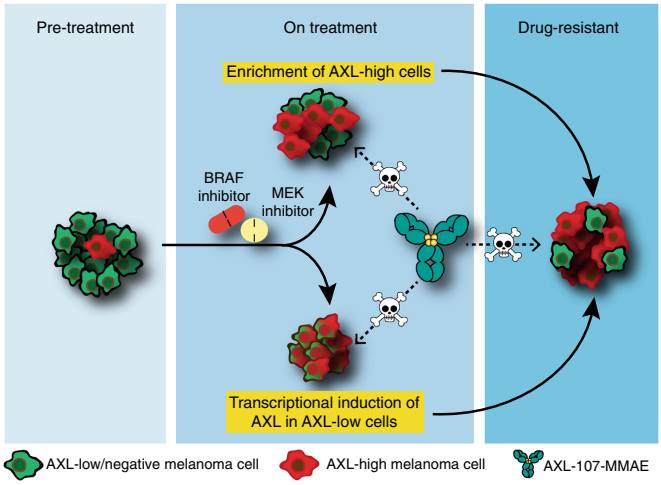

Figure 6 Eliminating heterogeneous melanoma by targeting distinct populations with AXL-107-MMAE and MAPK pathway inhibitors. Most melanomas display intratumor heterogeneity, as they already contain single or small groups of AXL-positive cells before treatment (left). When these tumors are treated with BRAF and/or MEK inhibitors, two processes occur: AXL-positive, drug-resistant cells become enriched (top middle), and AXL expression is acutely induced, also in AXL-low cells (bottom middle). The net effect of this is the accumulation of AXL-positive cells in treatment-refractory tumors (right). We found that AXL-107-MMAE targeted AXL-high cells at different phases during treatment: it eliminated AXL-high cells that were enriched following treatment (**Fig. 3**), previously AXL-low cells that upregulated AXL on treatment (**Fig. 4**) and cells that had acquired drug resistance (**Fig. 2**). We corroborated these findings in PDX models *in vivo* (**Fig. 5**). Thus, by targeting distinct populations, AXL-107-MMAE and MAPK pathway inhibitors cooperatively eliminate heterogeneous melanoma.

It has been suggested that, given the common heterogeneity of cancers, combination therapies targeting at least two different pathways are required to overcome cancer drug resistance and achieve more durable clinical responses[4]. Investigators have mechanistically dissected tumor responses to therapy in an effort to uncover and pharmacologically target compensatory pathways. For example, vemurafenib treatment of BRAF-mutant colorectal cancer causes feedback activation of EGFR signaling, which can be inhibited with EGFR inhibitors[53]. Similarly, trametinib has been shown to drive a compensatory FGFR1-dependent signal, which can be abolished by FGFR1 inhibitor[54]. Although those combinatorial approaches are likely to increase therapeutic effect, they are targeting only one tumor (sub) population, ignoring tumor heterogeneity. In contrast, we found that AXL-107-MMAE and MAPK pathway inhibitors target distinct populations in heterogeneous pools of melanoma cells; whereas AXL-107-MMAE eliminated MAPK pathway inhibitor-resistant, AXL-high tumor cell pools, MAPK pathway inhibitors killed AXL-low populations. Thus, AXL-107-MMAE and MAPK pathway inhibitors cooperatively inhibit tumor growth, constituting a rationalized approach to combinatorial targeting.

We also found that AXL-107-MMAE and MAPK pathway inhibitors cooperated in a dual fashion (**Fig. 6**). First, AXL-107-MMAE eliminated AXL-positive cells that were enriched under therapeutic pressure of MAPK inhibition to cause relapse of resistant tumors. Second, MAPK inhibitors caused acute transcriptional induction of AXL in previously AXL-low melanomas, increasing the efficacy of AXL-107-MMAE (in both BRAF- and NRAS-mutant tumors). The latter result extends previous data on MEK inhibitors influencing proteolytic shedding of several RTKs, including AXL[55]. Corroborating these mechanisms *in vivo*, we observed cooperative growth inhibition of treatment-naive and drug-resistant melanomas alike, both in PDX models comprising rare AXL-positive cells and those containing large groups of AXL-positive cells. Finally, we found that AXL-107-MMAE prevented the emergence of populations that resist MAPK pathway inhibitors.

AXL is expressed in multiple cancer types and, extending previous observations[24,30,31,38,56,57], we found that it is strongly associated with pan-cancer EMT. Furthermore, high AXL expression levels are associated with resistance to a plethora of drug therapies and drug combinations[17,26,29]. For those reasons, it is conceivable that targeting cancer cells that express this RTK will be a beneficial approach to eliminate invasive, drug-resistant cancer cells. Our data suggest that the benefit of targeting AXL-positive cells may even go beyond the setting of acquired drug resistance, as we found that AXL-positive cells, either alone or in small groups, commonly reside in pre-treatment melanomas, thereby corroborating recent single-cell analyses[58,59]. Thus, AXL-positive cells may constitute pre-existing drug-resistant reservoirs that expand during treatment, producing treatment-refractory tumor cell pools. We found that this was the case for both BRAF- and NRAS-mutant melanomas treated with BRAF and/or MEK inhibitors.

In conclusion, it is conceivable that the common heterogeneity of tumors is associated with subpopulations that show distinct therapy response profiles; we propose accordingly that these different populations should receive tailored treatments. As we found for melanomas, which commonly harbor pools of MAPK pathway inhibitor-resistant, AXL-high cells that are intermingled with those that are MAPK pathway inhibitor sensitive and AXL low, rationalized combinatorial targeting greatly improved therapeutic benefit. AXL-107-MMAE shows promising anti-tumor activity in preclinical, AXL-positive tumor models as a monotherapy. Furthermore, its activity can be leveraged in a combination setting with therapies that lead to increased AXL expression. On the basis of both these preclinical data and the non-clinical safety profile, the clinical safety and efficacy of AXL-107-MMAE are currently being evaluated in a phase 1/2 clinical study for various solid tumor indications, including ovarian cancer, NSCLC and melanoma (NCT02988817).

METHODS

Methods, including statements of data availability and any associated accession codes and references, are available in the online version of the paper.

Note: Any Supplementary Information and Source Data files are available in the online version of the paper.

ACKNOWLEDGMENTS

We thank all the members of the Peeper and Blank laboratories for their valuable input and the FACS facility and animal facility at the NKI for their support. We would like to acknowledge the NKI-AVL Core Facility Molecular Pathology & Biobanking (CFMPB) for supplying NKI-AVL Biobank material and lab support. We thank M. van der Ven and the intervention unit (NKI) for their help with animal experiments, M. Mertz and E. Gielen for their help with confocal microscopy, and H. Witteveen, M. Houtkamp, G. Rigter and T. Kroes for help with experiments. The research leading to these results has been funded by a grant from Genmab, by the European Research Council under the European Union's Seventh Framework Programme (FP7/2007-2013)/ERC synergy grant agreement n° 319661 COMBATCANCER and grants NKI 2014-7241, NKI 2013-5799 and NKI 2017-10425 from the Dutch Cancer Society (KWF).

AUTHOR CONTRIBUTIONS

J.B., L.A.K., E.C.W.B., M.L.J., D.S., D.S.P. and P.W.H.I.P. designed the study, analyzed the data and wrote the manuscript. J.B., M.A.L., D.W.V., N.P. and E.G.-v.d.H.

performed the experiments. O.K. performed the bioinformatics analyses. K.K. and D.S.P. developed the melanoma PDX-platform and engineered PDX-derived cell lines. A.S. and J.B. performed *in vivo* melanoma experiments. J.-Y.S. analyzed IHC from *in vivo* experiments. T.K. and C.U.B. gave critical input. J.T.M. directed toxicological analyses. M.G.F. and E.A.R. provided paired human melanoma samples. D.S.P. and P.W.H.I.P. supervised the study.

COMPETING FINANCIAL INTERESTS

The authors declare competing financial interests: details are available in the online version of the paper.

1. McGranahan, N. & Swanton, C. Clonal heterogeneity and tumor evolution: past, present, and the future. *Cell* **168**, 613–628 (2017).
2. Aparicio, S. & Caldas, C. The implications of clonal genome evolution for cancer medicine. *N. Engl. J. Med.* **368**, 842–851 (2013).
3. Sharma, P., Hu-Lieskovan, S., Wargo, J.A. & Ribas, A. Primary, adaptive, and acquired resistance to cancer immunotherapy. *Cell* **168**, 707–723 (2017).
4. Diaz, L.A. Jr. *et al.* The molecular evolution of acquired resistance to targeted EGFR blockade in colorectal cancers. *Nature* **486**, 537–540 (2012).
5. Long, G.V. *et al.* Combined BRAF and MEK inhibition versus BRAF inhibition alone in melanoma. *N. Engl. J. Med.* **371**, 1877–1888 (2014).
6. Robert, C. *et al.* Improved overall survival in melanoma with combined dabrafenib and trametinib. *N. Engl. J. Med.* **372**, 30–39 (2015).
7. Larkin, J. *et al.* Combined vemurafenib and cobimetinib in *BRAF*-mutated melanoma. *N. Engl. J. Med.* **371**, 1867–1876 (2014).
8. Flaherty, K.T. *et al.* Combined BRAF and MEK inhibition in melanoma with *BRAF* V600 mutations. *N. Engl. J. Med.* **367**, 1694–1703 (2012).
9. Chapman, P.B. *et al.* Improved survival with vemurafenib in melanoma with *BRAF* V600E mutation. *N. Engl. J. Med.* **364**, 2507–2516 (2011).
10. Long, G.V. *et al.* Factors predictive of response, disease progression, and overall survival after dabrafenib and trametinib combination treatment: a pooled analysis of individual patient data from randomised trials. *Lancet Oncol.* **17**, 1743–1754 (2016).
11. Smith, M.P. *et al.* The immune microenvironment confers resistance to MAPK pathway inhibitors through macrophage-derived TNFα. *Cancer Discov.* **4**, 1214–1229 (2014).
12. Nazarian, R. *et al.* Melanomas acquire resistance to B-RAF^{V600E} inhibition by RTK or N-RAS upregulation. *Nature* **468**, 973–977 (2010).
13. Girotti, M.R., Saturno, G., Lorigan, P. & Marais, R. No longer an untreatable disease: how targeted and immunotherapies have changed the management of melanoma patients. *Mol. Oncol.* **8**, 1140–1158 (2014).
14. Davies, M.A. & Samuels, Y. Analysis of the genome to personalize therapy for melanoma. *Oncogene* **29**, 5545–5555 (2010).
15. Shi, H. *et al.* Acquired resistance and clonal evolution in melanoma during BRAF inhibitor therapy. *Cancer Discov.* **4**, 80–93 (2014).
16. Kemper, K. *et al.* Intra- and inter-tumor heterogeneity in a vemurafenib-resistant melanoma patient and derived xenografts. *EMBO Mol. Med.* **7**, 1104–1118 (2015).
17. Müller, J. *et al.* Low MITF/AXL ratio predicts early resistance to multiple targeted drugs in melanoma. *Nat. Commun.* **5**, 5712 (2014).
18. Konieczkowski, D.J. *et al.* A melanoma cell state distinction influences sensitivity to MAPK pathway inhibitors. *Cancer Discov.* **4**, 816–827 (2014).
19. Leucci, E., Close, P. & Marine, J.-C. Translation rewiring at the heart of phenotype switching in melanoma. *Pigment Cell Melanoma Res.* **30**, 282–283 (2017).
20. Hoek, K.S. *et al.* Metastatic potential of melanomas defined by specific gene expression profiles with no BRAF signature. *Pigment Cell Res.* **19**, 290–302 (2006).
21. Hoek, K.S. *et al. In vivo* switching of human melanoma cells between proliferative and invasive states. *Cancer Res.* **68**, 650–656 (2008).
22. Elkabets, M. *et al.* AXL mediates resistance to PI3Kα inhibition by activating the EGFR/PKC/mTOR axis in head and neck and esophageal squamous cell carcinomas. *Cancer Cell* **27**, 533–546 (2015).
23. Reichl, P. *et al.* Axl activates autocrine transforming growth factor-β signaling in hepatocellular carcinoma. *Hepatology* **61**, 930–941 (2015).
24. Bansal, N., Mishra, P.J., Stein, M., DiPaola, R.S. & Bertino, J.R. Axl receptor tyrosine kinase is up-regulated in metformin resistant prostate cancer cells. *Oncotarget* **6**, 15321–15331 (2015).
25. Byers, L.A. *et al.* An epithelial-mesenchymal transition gene signature predicts resistance to EGFR and PI3K inhibitors and identifies Axl as a therapeutic target for overcoming EGFR inhibitor resistance. *Clin. Cancer Res.* **19**, 279–290 (2013).
26. Zhang, Z. *et al.* Activation of the AXL kinase causes resistance to EGFR-targeted therapy in lung cancer. *Nat. Genet.* **44**, 852–860 (2012).
27. Creedon, H. *et al.* Exploring mechanisms of acquired resistance to HER2 (human epidermal growth factor receptor 2)-targeted therapies in breast cancer. *Biochem. Soc. Trans.* **42**, 822–830 (2014).
28. Zhou, L. *et al.* Targeting MET and AXL overcomes resistance to sunitinib therapy in renal cell carcinoma. *Oncogene* **35**, 2687–2697 (2016).
29. Debruyne, D.N. *et al.* ALK inhibitor resistance in ALK^{F1174L}-driven neuroblastoma is associated with AXL activation and induction of EMT. *Oncogene* **35**, 3681–3691 (2016).
30. Wang, C. *et al.* Gas6/Axl axis contributes to chemoresistance and metastasis in breast cancer through Akt/GSK-3β/β-catenin signaling. *Theranostics* **6**, 1205–1219 (2016).
31. Kurokawa, M., Ise, N., Omi, K., Goishi, K. & Higashiyama, S. Cisplatin influences acquisition of resistance to molecular-targeted agents through epithelial-mesenchymal transition-like changes. *Cancer Sci.* **104**, 904–911 (2013).
32. Hong, C.-C. *et al.* Receptor tyrosine kinase AXL is induced by chemotherapy drugs and overexpression of AXL confers drug resistance in acute myeloid leukemia. *Cancer Lett.* **268**, 314–324 (2008).
33. Aguilera, T.A. *et al.* Reprogramming the immunological microenvironment through radiation and targeting Axl. *Nat. Commun.* **7**, 13898 (2016).
34. Bhang, H.-E.C. *et al.* Studying clonal dynamics in response to cancer therapy using high-complexity barcoding. *Nat. Med.* **21**, 440–448 (2015).
35. Hata, A.N. *et al.* Tumor cells can follow distinct evolutionary paths to become resistant to epidermal growth factor receptor inhibition. *Nat. Med.* **22**, 262–269 (2016).
36. Sharma, S.V. *et al.* A chromatin-mediated reversible drug-tolerant state in cancer cell subpopulations. *Cell* **141**, 69–80 (2010).
37. Turke, A.B. *et al.* Preexistence and clonal selection of *MET* amplification in *EGFR* mutant NSCLC. *Cancer Cell* **17**, 77–88 (2010).
38. Cichoń, M.A. *et al.* The receptor tyrosine kinase Axl regulates cell-cell adhesion and stemness in cutaneous squamous cell carcinoma. *Oncogene* **33**, 4185–4192 (2014).
39. Mak, M.P. *et al.* A patient-derived, pan-cancer EMT signature identifies global molecular alterations and immune target enrichment following epithelial-to-mesenchymal transition. *Clin. Cancer Res.* **22**, 609–620 (2016).
40. Garnett, M.J. *et al.* Systematic identification of genomic markers of drug sensitivity in cancer cells. *Nature* **483**, 570–575 (2012).
41. Loges, S. *et al.* Malignant cells fuel tumor growth by educating infiltrating leukocytes to produce the mitogen Gas6. *Blood* **115**, 2264–2273 (2010).
42. Adams, G.P. *et al.* High affinity restricts the localization and tumor penetration of single-chain fv antibody molecules. *Cancer Res.* **61**, 4750–4755 (2001).
43. Donaghy, H. Effects of antibody, drug and linker on the preclinical and clinical toxicities of antibody-drug conjugates. *MAbs* **8**, 659–671 (2016).
44. Chen, R. *et al.* CD30 downregulation, MMAE resistance, and MDR1 upregulation are all associated with resistance to brentuximab vedotin. *Mol. Cancer Ther.* **14**, 1376–1384 (2015).
45. Szakács, G., Paterson, J.K., Ludwig, J.A., Booth-Genthe, C. & Gottesman, M.M. Targeting multidrug resistance in cancer. *Nat. Rev. Drug Discov.* **5**, 219–234 (2006).
46. Holderfield, M., Deuker, M.M., McCormick, F. & McMahon, M. Targeting RAF kinases for cancer therapy: *BRAF*-mutated melanoma and beyond. *Nat. Rev. Cancer* **14**, 455–467 (2014).
47. Kemper, K. *et al.* BRAF^{V600E} kinase domain duplication identified in therapy-refractory melanoma patient-derived xenografts. *Cell Rep.* **16**, 263–277 (2016).
48. de Goeij, B.E. & Lambert, J.M. New developments for antibody-drug conjugate–based therapeutic approaches. *Curr. Opin. Immunol.* **40**, 14–23 (2016).
49. Thomas, A., Teicher, B.A. & Hassan, R. Antibody-drug conjugates for cancer therapy. *Lancet Oncol.* **17**, e254–e262 (2016).
50. Asundi, J. *et al.* MAPK pathway inhibition enhances the efficacy of an anti–endothelin B receptor drug conjugate by inducing target expression in melanoma. *Mol. Cancer Ther.* **13**, 1599–1610 (2014).
51. Breij, E.C.W. *et al.* An antibody-drug conjugate that targets tissue factor exhibits potent therapeutic activity against a broad range of solid tumors. *Cancer Res.* **74**, 1214–1226 (2014).
52. Doronina, S.O. *et al.* Development of potent monoclonal antibody auristatin conjugates for cancer therapy. *Nat. Biotechnol.* **21**, 778–784 (2003).
53. Prahallad, A. *et al.* Unresponsiveness of colon cancer to BRAF^{V600E} inhibition through feedback activation of EGFR. *Nature* **483**, 100–103 (2012).
54. Manchado, E. *et al.* A combinatorial strategy for treating *KRAS*-mutant lung cancer. *Nature* **534**, 647–651 (2016).
55. Miller, M.A. *et al.* Reduced proteolytic shedding of receptor tyrosine kinases is a post-translational mechanism of kinase inhibitor resistance. *Cancer Discov.* **6**, 382–399 (2016).
56. Creedon, H. *et al.* Identification of novel pathways linking epithelial-to-mesenchymal transition with resistance to HER2-targeted therapy. *Oncotarget* **7**, 11539–11552 (2016).
57. Xu, W. *et al.* Up-regulation of the Hippo pathway effector TAZ renders lung adenocarcinoma cells harboring *EGFR*-T790M mutation resistant to gefitinib. *Cell Biosci.* **5**, 7 (2015).
58. Tirosh, I. *et al.* Dissecting the multicellular ecosystem of metastatic melanoma by single-cell RNA-seq. *Science* **352**, 189–196 (2016).
59. Shaffer, S.M. *et al.* Rare cell variability and drug-induced reprogramming as a mode of cancer drug resistance. *Nature* **546**, 431–435 (2017).

ONLINE METHODS

Generation of human AXL-specific monoclonal antibodies. Human immunoglobulin G (IgG)-1κ AXL-specific monoclonal antibodies (AXL HuMab) were generated by immunization of HuMab mice[60] (Medarex) with his-tagged AXL-ECD protein, AXL-FN2-ECD protein, AXL-Ig12-ECD protein and/or EL4 cells transfected with full length human AXL. Hybridomas were generated from mice that showed AXL-specific antibodies in serum, as assessed by binding to AXL expressing cell lines A431 (DSMZ), MDA-MB-231 (ATCC), and HEK293 cells transiently expressing full length human AXL using Fluorimetric Microvolume Assay Technology (Applied Biosystems). Binding to HEK293 wild-type cells, which do not express AXL, was included as a negative control. Hybridomas producing AXL-specific HuMab were identified by screening culture supernatants as described above. To determine the antibody variable region sequences of AXL-specific HuMab, mRNA was extracted from selected hybridomas and the immunoglobulin variable heavy and light chain regions were amplified, cloned, and sequenced. Recombinant antibodies were generated as described[61], and the recombinant IgG1κ was used for further characterization of the AXL HuMab. The IgG1κ antibody IgG1-b12, that binds to HIV glycoprotein gp120 (ref. 62), was included as isotype control antibody.

For antibodies AXL-154, AXL-183 and AXL-726, the following variants with point mutations in the variable domains were generated by site-directed mutagenesis using the Quickchange II mutagenesis kit (Stratagene): AXL-154-M103L, AXL-183-N52Q and AXL-726-M101L to avoid posttranslational modifications such as methionine oxidation and N-linked glycosylation in the Fab domain.

Of the diverse panel of 11 antibodies (**Supplementary Table 1**), 9 AXL-antibodies and the isotype control IgG1-b12 were conjugated with Maleimidocaproyl-valine-citrulline-p-aminobenzoyloxycarbonyl-monomethyl auristatin E containing a protease-cleavable valine-citrulline dipeptide as described[52]. The average drug-antibody ratio was 4:1.

Binding of AXL antibodies to AXL, MER and TYRO3-expressing cells. Binding of AXL human mAb AXL-107 and AXL-107-MMAE to AXL-expressing HEK293 cells, transiently transfected with expression constructs for full length human AXL, MER and TYRO3, was evaluated by flow cytometry. Proper expression of MER and TYRO3 was confirmed using mouse-anti-human antibodies for MER and TYRO3 (mouse anti-human MER, R&D Systems, cat. No. MAB8912; mouse anti-human TYRO3, R&D Systems, cat. No. MAB859) and anti-mouse IgG FITC (Dako, cat. No. F0479).

Binding affinity of AXL antibodies. Binding affinities were determined using BioLayer Interferometry on a ForteBio OctetRED384. Anti-human Fc Capture biosensors were loaded for 150 s with AXL antibodies aiming at a loading response of 1 nm. After a baseline (150 s) the association (1,000 s) and dissociation (2,000 s) of AXL-ECDHis (the extracellular domain [ECD] of human AXL [aa 1–447] with a C-terminal His tag) was determined.

Mapping of the antibody binding domain. The AXL domain specificity of the AXL antibodies was determined using a panel of human-mouse chimeric AXL variants. Five different chimeric AXL molecules were generated, in which either the entire human extracellular domain, the human Ig-like domain I (Ig1), the Ig-like domain II (Ig2), the human FNIII-like domain I (FN1) or the human FNIII-like domain II domain (FN2) were replaced with their mouse homologs. Antibody binding was determined by flow cytometry.

Gas6 competition. AXL-positive A431 cells were incubated with 10 μg/ml recombinant human Gas6 for 15 min at 4 °C. Binding of AXL antibodies was evaluated by flow cytometry using an R-Phycoerythrin (PE)-conjugated goat-anti-human IgG F(ab')2 (Jackson ImmunoResearch Laboratories; cat. No. 109-116-098) as detection reagent. Cells were analyzed on a FACS Canto II (BD Biosciences).

Antibody internalization. AXL antibodies or IgG1-b12 (1.5 μg/ml) were complexed with goat-anti-human Fab-fragments (Jackson Immunoresearch) conjugated with the fluorophore and quencher pair TAMRA/QSY7 (12 μg/ml; 30 min, 4 °C), as described previously[51]. The complex was added to AXL-expressing LCLC-103H cells and incubated for 24 h in the dark, under shaking conditions (200 rpm, 37 °C). Upon internalization and degradation of the complex, dissociation of TAMRA and QSY results in dequenching of TAMRA. The resulting fluorescent signal was measured on a FACS Canto-II (BD Biosciences).

Nonclinical safety study. The potential cross-reactivity of AXL-107-MMAE with a selected panel of human and cynomolgus monkey tissues was assessed by Covance Laboratories using FITC-labeled AXL-107-MMAE. The dose toxicity study in mature cynomolgus monkeys was performed by Charles River Laboratories Edinburgh. This study, with the exception of bioanalysis and antidrug antibody analysis, was performed in accordance with the OECD Principles of Good Laboratory Practice (GLP).

***In vivo* tumor induction, treatment and response analysis of PDX models CV1664, LXFA526.** The anti-tumor activity of AXL-107-MMAE, AXL-148-MMAE, and AXL-733-MMAE was determined in the pancreas cancer patient-derived xenograft (PDX) model PAXF1657. Experiments were performed by Oncotest. The further *in vivo* therapeutic activity of 107-AXL-MMAE was tested in xenograft tumor models derived from patient-derived primary tumors (PDX) in nude mice at Crown Biosciences and Charles River Discovery Research Services Germany (GmbH). Mice were inoculated subcutaneously at the right flank with one tumor fragment (2–3 mm diameter). Tumor volumes were measured at least twice per week using a digital caliper (PLEXX). Tumor volumes (mm^3) were calculated as follows: tumor volume = 0.52 × (length) × $(width)^2$. Before treatment, mice were divided into groups of 6–8 mice each, with equal tumor size distribution (average and variance). Randomization occurred in a blinded fashion. Mice were treated intraperitoneally or intravenously with approximately 0.2 ml test solution per mouse, adjusted to actual body weight, according to the schedule specified at each experiment. Body weight of the mice was monitored twice weekly. Mice were observed at least three times weekly for clinical signs of illness. The experiment ended for individual mice either when the tumor size exceeded 1.5 cm^3, the tumor showed ulceration, in case of serious clinical illness, when the tumor growth blocked the movement of the mouse, or when tumor growth assessment had been completed. Differences in mean tumor volumes were compared between treatment groups using one-way ANOVA. Mantel-Cox analysis of Kaplan-Meier curves was performed to analyze statistical differences in progression-free survival time with a general tumor-size cut-off of 500 mm^3.

Protocols and any amendment(s) or procedures involving the care and use of animals in the studies were reviewed and approved by the Institutional Animal Care and Use Committee (IACUC) of Crown Biosciences, and by the local authorities of the "Regierungspraesidium Freiburg" in case of Charles River Discovery Research Services Germany GmbH, Freiburg, Germany before conduct. During the study, the care and use of animals was conducted in accordance with the regulations of the Association for Assessment and Accreditation of Laboratory Animal Care (AAALAC).

***In vivo* tumor induction, treatment and response analysis of melanoma cell lines.** The *in vivo* therapeutic activity of 107-AXL-MMAE in melanoma cell lines was tested in nude mice at NKI. Mice were inoculated subcutaneously at the right flank with 0.25–1 × 10^6 cells. Tumor size was measured twice weekly with a caliper and tumor volume was calculated using the following formula: ½ × length (mm) × width (mm). Randomization occurred in a blinded fashion. When tumors reached 100 mm^3, mice were distributed in groups of 6–8 each, with equal tumor sizes. Mice were treated intravenously with 0.1 ml ADC solution per mouse, according to the schedule specified at each experiment. Dabrafenib (GSK211436) and trametinib (GSK1120212) were given daily orally at doses of 30 mg/kg and 0.3 mg/kg, respectively, dissolved in 0.5% hydroxypropylmethylcellulose (Sigma), 0.2% Tween-80 (Sigma) in distilled water (HPMC) to a final volume of 300 μl/mouse. Start of oral gavage occurred concurrently with the first day of injection of the ADCs. The experiment ended for individual mice either when the tumor size exceeded 1.5 cm^3, the tumor showed ulceration, in case of serious clinical illness, when the tumor growth blocked the movement of the mouse, or when tumor growth assessment had been completed. Mantel-Cox analysis of Kaplan-Meier curves was performed to analyze statistical differences in progression-free survival time with a general tumor-size cut-off of 500–800 mm^3.

Patient samples, animals for melanoma studies and melanoma PDX-derived xenograft models. The collection and use of human tissue was approved by the Medical Ethical Review Board of the Antoni van Leeuwenhoek. Animal experiments were approved by the animal experimental committee of the institute and performed according to Dutch law. Melanoma PDX-derived xenograft models were derived as described previously[47].

Melanoma PDX-derived cell lines. After resection from mice, melanoma PDX were cut into small pieces by mechanical dissociation. Tumor pieces were incubated for 30 min at 37 °C with 1:100 collagenase IV (17104-019, Invitrogen) and 1:100 DNAse (07900, Bio-Connect) in serum-free DMEM to obtain single-cell suspensions. By passing the mixture through a 70-µm filter, single cells were plated on 10-cm dishes. Through serial passaging of the tumor cells, cell lines were obtained.

Immunohistochemistry of tumor tissues. AXL immunohistochemistry was performed using the following protocol: after xylene treatment (3 × 5 min), antigen retrieval on FFPE material was performed using citrate buffer (pH 6) in a pressure cooker for 5 min. Staining was performed either manually (melanoma) in Sequenza Slide Racks (Ted Pella; cat. no. 36105) or on a Ventana BenchMark Ultra (IHC Autostainer) for other tumor tissues. Sections were blocked in 10% human serum (NHS) in PBS-T for 30 min, and primary antibody AXL (sc-20471) at a concentration of 1–3 µg/ml was incubated for 60 min in 2% NHS in PBS-T. Detection antibody was poly-HRP-anti-rabbit (Immunologic Brightvision) and stainings were developed using 3,3′-diaminobenzidine (DAB) chromophore (DAKO, cat. no. K3468) or, in the case of melanoma tissues, AEC chromophore (red color; Sigma, cat. no. A6926-100TAB), to be able to distinguish between brown melanin pigment and specific staining. A counterstain of hematoxylin was applied. Slides of CDX/PDX models of various tumor types were analyzed and scored with quantitative image analysis using Definiens Tissue Studio (TS) software (version 4.1; Definiens). Using this software, immunostained tissue sections were analyzed for the percentage of tumor cells expressing AXL and AXL staining intensity (brown chromogen intensity) per cell. Melanoma tissue slides were manually analyzed and scored by a certified pathologist from the VU University Medical Center, in a blinded fashion. Melanoma cells were identified by histopathological features. Percentage AXL-positive melanoma cells staining weak (1+), moderate (2+) or strong (3+) were assessed in 10% intervals. Tumor tissues were considered AXL-positive if AXL expression was observed in at least 10% of tumor cells. Staining intensity and percentage positive tumor cells were combined as AXL H-score according to the following formula: H-score = (1 × % 1+ tumor cells) + (2 × % 2+ tumor cells) + (3 × % 3+ tumor cells).

Inhibitors and solvents. MEK inhibitor GSK1120212/trametinib, BRAF inhibitors PLX4720, PLX4032/vemurafenib and GSK211436/dabrafenib were all purchased from Selleck Chemicals. The metabolic poison phenyl arsine oxide (PAO) and solvent dimethyl- sulfoxide were from Sigma-Aldrich. All drugs were reconstituted in 100% dimethylsulfoxide to a final concentration of 1–10 mM. For all AXL induction experiments and co-cultures, dabrafenib was used at 1 µM and trametinib was used at 0.1 µM. For all co-culture experiments, AXL-107-MMAE was used at 1 µg/ml.

Western blotting and antibodies. Cell pellets were lysed in RIPA buffer (50 mM TRIS pH 8.0, 150 mM NaCl, 1% Nonidet P40, 0.5% sodium deoxycholate, 0.1% SDS) supplemented with complete protease inhibitor cocktail (Roche Applied Science) and phosphatase inhibitors 10 mM NaF, 1 mM Na_3VO_4, 1 mM sodium pyrophosphate, 10 mM beta-glycerophosphate. Protein concentration was determined with the BCA Protein Assay Kit (Pierce). Western blotting was performed with standard techniques using 4–12% Bis-Tris polyacrylamide-SDS gels (NuPAGE, Life Technologies) and nitrocellulose membranes (Whatman, GE Healthcare). Blots were blocked in 4% milk in PBS plus 0.2% Tween 100 and incubated with primary antibody: AXL (1:1,000, sc-20741), purchased from Santa Cruz; β-actin (1:10.000, AC-74) purchased from Sigma; vinculin (1:10,000, V9131-100UL, Sigma) and GAPDH (1:1000, sc-69778, Santa Cruz). The following secondary antibodies were used: goat anti-rabbit peroxidase conjugate (1:5,000, G21234) and goat anti-mouse (1:5,000, G21040), both purchased from Invitrogen. Western blots were incubated in a 1:1 dilution of solution 1 (0.1 M Tris pH 8, 2.5 mM luminol, 0.4 mM p-Coumaric acid, all Sigma) and solution 2 (0.1 M Tris pH 8, 30% H_2O_2, all Sigma) and chemiluminescent signal was visualized using high performance autoradiography films (Hyperfilm MP, Amersham).

Melanoma cell lines, cell culture conditions and transfections. Melanoma cell lines and HEK293T cells were cultured in DMEM with fetal bovine serum (Sigma), 100 U/ml penicillin and 0.1 mg/ml streptomycin (all Gibco) under standard conditions. HEK293T cells were used for virus production for fluorescent labeling and shAXL experiments of cell lines. In brief, HEK293T cells were transfected with the plasmid of interest (pCDH-mCherry, pLX304-GFP or shAXL) and the helper plasmids psPAX and MS2G (Addgene). Viral supernatant was either snap frozen or immediately used for infection. Infected melanoma cells were fluorescence-sorted with FACS Aria III (fluorescent labels) or puromycin-selected (shAXL). Sequences for shAXL were 1: 5′ CCGGCGTGGAGAACAGCGAGATTTACTCGAGTAAATCTCGCTGTTCTCCACGTTTTTTG and 2: 5′CCGGCCTAAGCATCTAAGTTATAAGCTCGAGCTTATAACTTAGATGCTTAGGTTTTTTG.

Generation of MAPK-pathway-inhibitor-resistant melanoma cell lines. BRAF inhibitor-resistant and MEK inhibitor-resistant cell lines were previously generated in the lab, by exposing to PLX4720 (up to 3 µM) or trametinib (GSK1120212) (up to 0.1 µM)[17]. Resistance was confirmed by measuring cell viability under treatment. BRAF inhibitor-resistant cell line SkMel-28-R was permanently cultured under 3 µM of PLX4720, and MEK inhibitor-resistant cell line SkMel-2-R was permanently cultured under 0.1 µM of trametinib.

***In vitro* cytotoxicity assays with AXL antibodies and AXL-107-MMAE.** All cell lines except melanoma were seeded at 1×10^3 cells per well in 96 well culture plates (Greiner) and incubated for 3 h at 37 °C, 5% CO_2 to allow adherence to the plate. Subsequently, serial dilutions (fourfold; final concentrations ranging from 10 to 0.00015 µg/ml) of unconjugated, MMAE-conjugated AXL antibodies or an MMAE-conjugated isotype control antibody (IgG1-b12-MMAE) were prepared in culture medium and added to the plates. Free MMAE –monomethyl auristatin E (MMAE, licensed from Seattle Genetics) was used at a start concentration of 718 ng/ml in fourfold dilution series. Incubation of cells with 1 µM staurosporin (S6942-200, Sigma) was used as reference for 100% tumor cell kill. Untreated cells were used as reference for 0% tumor cell kill. After 5 d, Cell TiterGlo Reagent (Promega, cat.no G7571) was added to the wells (20 µl, or 10% of total well volume) and plates were incubated for 1.5 h at 37 °C, 5% CO2. Subsequently, 120 µl per well was transferred to white 96-well Optiplate plates (PerkinElmer; cat.no. 6005299), and incubated for 30 min at 21 °C. Finally, luminescence was measured on an EnVision multiplate reader (Envision, Perkin Elmer). For dose-response curves and viability assays in melanoma, 1×10^3 cells were plated in 96-well plates and ADC was added 3 h after seeding with the HP D300 Digital Dispenser (Tecan). After 5 d of incubation, the medium was replaced by a dilution of CellTiter Blue (Promega) in medium. Fluorescence was measured by the Infinite M200 microplate reader (Tecan) after 3 h. The percentage of living cells was calculated using the following equation, where RLU represent relative luminescence units: % living cells = (RLUADC – RLUstauro)/(RLUuntreated – RLUstauro) × 100%.

TCGA pan-cancer AXL expression. TCGA gene expression data was downloaded using the R/Bioconductor package 'TCGAbiolinks'[63] as FPKM values for each 32 tumor types. Gene expression for a set of 76 genes (24 upregulated in epithelial cells and 52 upregulated in mesenchymal cells)[39] was applied to determine EMT status. Gene expression was plotted in a heat map sorted according to the ratio of the average expression of genes upregulated in epithelial versus the gene upregulated in mesenchymal cells. To determine the correlation of AXL expression with EMT the FPKM expression values for AXL were sorted according to the EMT profile. A LOESS curve was fitted with a span of 0.4. Significance of correlation was assessed using $r = 0.65$ and samples size of 11,093.

GSEA. All protein coding genes for the complete pan-cancer TCGA cohort and COSMIC database were selected. Genes were pre-ranked based on the 'Spearman' correlation coefficient with AXL. GSEA, using the pre-ranked

doi:10.1038/nm.4472

genes, was run using the BROAD javaGSEA standalone version (http://www.broadinstitute.org/gsea/downloads.jsp) with the 52 mesenchymal genes as the GSEA gene set.

MDR1 mRNA quantification. RNA was extracted from whole-cell lysates using a total RNA isolation kit (RNeasy Mini Kit, 74106, Qiagen). 2 µg of total RNA was reverse transcribed into cDNA using the SuperScript VILO cDNA Synthesis Kit (11754-050, Invitrogen), and 5 µl of 1:64 diluted cDNA product was then mixed with 12.5 µl of the iQ Supermix (1708862, Bio-Rad), 1.25 µl of the respective 20× TaqMan assay (MDR1 [Hs00184500_m1] or ACTB [Hs99999903_m1]), and 6.25 µl of water for a total reaction volume of 25 µl. Real-time quantitative PCR (RT-qPCR) amplification was performed using a 96-well plate system (Bio-Rad qPCR system). Each PCR reaction was carried out in triplicates. MDR1 mRNA expression was normalized to β-actin (ACTB) mRNA expression.

AXL mRNA quantification. RNA was extracted using Isolate II RNA Mini Kit (Bioline) and 1 µg of total RNA was reverse transcribed into cDNA using Maxima First Strand cDNA kit (Thermo Scientific). The following primers were used for AXL: F-> 5′GGTGGCTGTGAAGACGATGA, R-> 5′CTCAGATACTCCATGCCACT. RPL13 was used as control housekeeping gene. Real-time quantitative PCR (RT-qPCR) amplification was performed using a 96-well plate system (Licor).

Knockout of MDR1 in NCI-H1299 cells. To inactivate MDR1 expression in H1299 lung cancer cells, a CRISPR-Cas9 lentiviral single-vector system was used (CVCRC-PX, Cellecta). Lentiviral particles were produced by transfecting 1.5×10^6 293T cells with ready-to-use lentiviral plasmid packaging mix (CPCP-K2A, Cellecta), 1.2 µg of plasmid (CRISPR-Cas9 one-vector plasmid containing a sgRNA against MDR1 or a control non-targeting sgRNA), and 9 µL of Lipofectamine 2000 transfection reagent (11668-027, Invitrogen). The media was refreshed 24 h after transfection, and the virus-containing media was harvested 72 h post-transfection. The virus-containing media was filtered through a 0.2-µm filter. The filtered undiluted virus-containing media was then used to transduce 0.5×10^6 H1299 cells in the presence of polybrene (8 µg/ml) for 6 h, after which the cell media was refreshed. Polyclonal puromycin selection (2 µg/ml) for cells that had successfully integrated the CRISPR-Cas9 plasmid was carried out 72 h post-transduction. The following sgRNA sequences were used:

sgMDR1-1:
5′ACCGATTGACAGCTATTCGAAGAGGTTTAAGAGCTATGCTGGAAACAGCATAGCAAGTTT 5′AAATAAGGCTAGTCCGTTATCAACTTGAAAAAGTGGCACCGAGTCGGTGCTTTTTTCG

sgMDR1-2: 5′ACCGCTGGAGAGATCCTCACCAAGGTTTAAGAGCTATGCTGGAAACAGCATAGCAAG 5′TTTAAATAAGGCTAGTCCGTTATCAACTTGAAAAAGTGGCACCGAGTCGGTGCTTTTTTCG

sgNon-Targeting: 5′ACCGGGCAGTCGTTCGGTTGATATGTTTAAGAGCTATGCTGGAAACAGCATAGCAAG 5′TTTAAATAAGGCTAGTCCGTTATCAACTTGAAAAAGTGGCACCGAGTCGGTGCTTTTTTCG

Flow cytometry. Cells were stained with AXL-PE conjugated antibody (1:50, FAB154P, R&D) for 1 h at 4C and analyzed at LSRII or LSR Fortessa (BD Bioscience). For quantification of AXL expression on the cell surface, Qifi quantification kit was used according to manufacturer's instructions (DAKO). In brief, cells were stained with isotype control IgG1 (MA110406, Pierce) or AXL antibody (1:100, ab89224, Abcam). Secondary antibody from the Qifi kit was used (Goat-α-mouse FITC). The number of AXL molecules on each cell was calculated using calibration beads from the Qifi kit according to according to manufacturer's instructions.

Microscopy. For confocal microscopy (**Supplementary Fig. 2k**), NCI-H1299 and LCLC-103H cells were seeded on 16-mm diameter coverslips in 12-well plates, at 40,000 and 30,000 cells per well, respectively. After 4 h, cells were incubated with leupeptin (50 µg/ml) for 30 min at 37 °C. Next, AXL-107 or the IgG1-b12 isotype control antibody (1 µg/ml) was added for 1- or 16-h incubations. Then, slides were rinsed twice with PBS and fixed for 30 min with 4% paraformaldehyde at 21 °C and washed with PBS. PFA signal was quenched by incubation with blocking buffer (1× PBS, 0.1% Saponin, 2% BSA and H_2O) and 20mM NH_4Cl for 20 min at 21 °C in the dark, all preceding steps were done in 400 µl volume. Slides were then washed two times with 300 µl blocking buffer, before staining with 300 µl goat-anti-human IgG F(ab′)2-FITC (1:150, Jackson ImmunoResearch, stock 1.0 mg/ml) and mouse-anti-human LAMP3-APC (1:50, BD Pharmingen, stock 0.05 mg/ml) for 45 min at 21 °C. Slides were washed with 1 ml of blocking buffer. For nuclear staining, slides were incubated for 5 min at 21 °C with 400 µl Hoechst (1:10,000 in PBS). To remove excessive Hoechst, slides were washed twice with 1 ml PBS. Furthermore, to remove possible salty deposits, slides were dipped in Aqua Braun and excess fluid was drained on tissue paper. Slides were then mounted on microscopic glasses for 4 h at 21 °C using 6 µl of Mowiol mounting medium (Cat. 475904, Lot. B52037, Man. Calbiochem). Confocal images were acquired on a Leica SP5 confocal microscope with a 63× 1.40 NA oil objective. All images were restored with Huygens Professional deconvolution software (SVI) and analyzed with the Huygens co-localization tool. The colocalization of 'fluorophores' (FITC and APC) was quantified using the Pearson's correlation coefficient. At least 15 cells were analyzed for each treatment.

For live-cell imaging (**Fig. 3g**), Incucyte technology (Essen Bioscience) was used to image and analyze the data. Red confluence was used as primary readout for mCherry-positive cells.

Statistical testing. The data of *in vivo* experiments were analyzed at the indicated time points in legends by Mann–Whitney test for non-parametrical analyses for two conditions, or one-way ANOVA, combined with Dunnett's multiple corrections test or Kruskal–Wallis test for non-parametrical analyses when >2 conditions were compared. Survival analyses on Kaplan–Meier curves was analyzed using Log-Rank Mantel–Cox test. All analyses were performed using the Prism Graphpad software. The data of *in vitro* experiments on melanoma cell lines were analyzed using the non-parametric tests Mann-Whitney for 2 conditions or Kruskal–Wallis test for >2 conditions.

Life Sciences Reporting Summary. Further information on experimental design is available in the **Life Sciences Reporting Summary**.

Data availability. TCGA gene expression data was downloaded from the The National Cancer Institute (NCI) Genomic Data Commons (GDC) database using the R/Bioconductor package 'TCGAbiolinks'[63]. BROAD javaGSEA standalone version can be downloaded from http://www.broadinstitute.org/ gsea/downloads.jsp.

60. Fishwild, D.M. *et al.* High-avidity human IgG κ monoclonal antibodies from a novel strain of minilocus transgenic mice. *Nat. Biotechnol.* **14**, 845–851 (1996).
61. Vink, T., Oudshoorn-Dickmann, M., Roza, M., Reitsma, J.-J. & de Jong, R.N. A simple, robust and highly efficient transient expression system for producing antibodies. *Methods* **65**, 5–10 (2014).
62. Burton, D.R. *et al.* Efficient neutralization of primary isolates of HIV-1 by a recombinant human monoclonal antibody. *Science* **266**, 1024–1027 (1994).
63. Colaprico, A. *et al.* TCGAbiolinks: an R/Bioconductor package for integrative analysis of TCGA data. *Nucleic Acids Res.* **44**, e71 (2016).

nature research

Corresponding author(s): D.S. Peeper

☐ Initial submission ☐ Revised version ☒ Final submission

Life Sciences Reporting Summary

Nature Research wishes to improve the reproducibility of the work that we publish. This form is intended for publication with all accepted life science papers and provides structure for consistency and transparency in reporting. Every life science submission will use this form; some list items might not apply to an individual manuscript, but all fields must be completed for clarity.

For further information on the points included in this form, see Reporting Life Sciences Research. For further information on Nature Research policies, including our data availability policy, see Authors & Referees and the Editorial Policy Checklist.

Experimental design

1. Sample size

Describe how sample size was determined.

Sample size was usually determined using the program G*Power. This included the upfront determination of the statistical tests that need to be used: e.g. a comparison between two groups was tested using Mann-Whitney, whereas comparison between multiple groups was performed using e.g. Kruskal-Wallis test. For other in vitro experiments we performed at least n=2-3 biological replicates for all experiments and on those groups that were to be analyzed by Kruskal-Wallis, we expanded these to at least n=5-6 replicates because of the multiple comparisons that had to be made.

2. Data exclusions

Describe any data exclusions.

Mice from in vivo experiments were excluded if they were sacrificed due to other reasons than the endpoint of the experiment (i.e. tumor volume), e.g. because of unrelated health issues for which action had to be undertaken (according to Dutch and international law).

3. Replication

Describe whether the experimental findings were reliably reproduced.

All attempts at replication were successful.

4. Randomization

Describe how samples/organisms/participants were allocated into experimental groups.

Allocation of mice was random and was performed by an independent technician. He/she assigned mice to different groups in a random fashion.

5. Blinding

Describe whether the investigators were blinded to group allocation during data collection and/or analysis.

Tumor measurements were performed by an independent technician without knowledge of group allocation. Also for IHC scoring the pathologist was blinded to the treatments the patients had received for which the biopsies were stained.

Note: all studies involving animals and/or human research participants must disclose whether blinding and randomization were used.

Nature Medicine: doi:10.1038/nm.4472

6. Statistical parameters

For all figures and tables that use statistical methods, confirm that the following items are present in relevant figure legends (or in the Methods section if additional space is needed).

n/a	Confirmed
☐	☒ The exact sample size (*n*) for each experimental group/condition, given as a discrete number and unit of measurement (animals, litters, cultures, etc.)
☐	☒ A description of how samples were collected, noting whether measurements were taken from distinct samples or whether the same sample was measured repeatedly
☐	☒ A statement indicating how many times each experiment was replicated
☐	☒ The statistical test(s) used and whether they are one- or two-sided (note: only common tests should be described solely by name; more complex techniques should be described in the Methods section)
☐	☒ A description of any assumptions or corrections, such as an adjustment for multiple comparisons
☐	☒ The test results (e.g. *P* values) given as exact values whenever possible and with confidence intervals noted
☐	☒ A clear description of statistics including central tendency (e.g. median, mean) and variation (e.g. standard deviation, interquartile range)
☐	☒ Clearly defined error bars

See the web collection on statistics for biologists for further resources and guidance.

Software

Policy information about availability of computer code

7. Software

Describe the software used to analyze the data in this study.

Graphpad Prism 7 was used to analyze the data.

For manuscripts utilizing custom algorithms or software that are central to the paper but not yet described in the published literature, software must be made available to editors and reviewers upon request. We strongly encourage code deposition in a community repository (e.g. GitHub). *Nature Methods* guidance for providing algorithms and software for publication provides further information on this topic.

Materials and reagents

Policy information about availability of materials

8. Materials availability

Indicate whether there are restrictions on availability of unique materials or if these materials are only available for distribution by a for-profit company.

AXL-107-MMAE is only available for distribution by a for-profit company (Genmab). PDX-derived melanoma tumors and cell lines can be provided on request to D.S. Peeper under collaboration agreements.

9. Antibodies

Describe the antibodies used and how they were validated for use in the system under study (i.e. assay and species).

For Western Blot:
AXL (1:1,000, sc-20741, Santa Cruz), confirmed for WB:https://www.citeab.com/antibodies/806105-sc-20741-axl-antibody-h-124
B-actin (1:10.000, AC-74, Sigma), confirmed for WB, https://www.sigmaaldrich.com/catalog/product/sigma/a2228?lang=en&region=NL
vinculin (1:10,000, V9131-100UL, Sigma), Confirmed for WB: https://www.sigmaaldrich.com/catalog/product/sigma/v9131?lang=en&region=NL
GAPDH (1:1000, sc-69778, Santa Cruz), confirmed for WB, https://www.scbt.com/scbt/product/gapdh-antibody-7b
goat anti-rabbit peroxidase conjugate (1:5,000, G21234, Invitrogen)
goat anti-mouse (1:5,000, G21040, Invitrogen), both specifically confirmed for WB:https://www.thermofisher.com/antibody/product/Goat-anti-Rabbit-IgG-H-L-Cross-Adsorbed-Secondary-Antibody-Polyclonal/G-21234

For IHC:
AXL (1:70, sc-20741, Santa Cruz), confirmed for IHC: https://www.citeab.com/antibodies/806105-sc-20741-axl-antibody-h-124 and confirmed in-house with RNA scope comparison for specificity.

Nature Medicine: doi:10.1038/nm.4472

10. Eukaryotic cell lines

a. State the source of each eukaryotic cell line used.

Cell lines were available from ATCC or derived from our melanoma PDX platform (Kemper et al. 2016). In vivo experiments at Crown Biosciences and Oncotest GmbH were performed using their cohorts of tumor models.

b. Describe the method of cell line authentication used.

Cell lines were STR profiled and confirmed to be authentic.

c. Report whether the cell lines were tested for mycoplasma contamination.

Cell lines were regularly tested and found to be mycoplasma-negative.

d. If any of the cell lines used are listed in the database of commonly misidentified cell lines maintained by ICLAC, provide a scientific rationale for their use.

No commonly mis-identified cell lines were used.

Animals and human research participants

Policy information about studies involving animals; when reporting animal research, follow the ARRIVE guidelines

11. Description of research animals

Provide details on animals and/or animal-derived materials used in the study.

Female NMRI-nude mice, age 6-8 weeks, were used for mouse experiments. Male and female cynomolgus monkeys were used for the non-clinical safety studies.

Policy information about studies involving human research participants

12. Description of human research participants

Describe the covariate-relevant population characteristics of the human research participants.

The study did not involve any human research participants. Only tumor biopsy analysis was performed on archive material, for which informed consent was given.

Nature Medicine: doi:10.1038/nm.4472